Supporting information

Insight into structural and energetic features of substituted triazolofurazans

Sofya P. Balabanova,[a] Alexey A. Voronin,*[a] Alexandr M. Churakov,*[a] Michael S. Klenov,[a] Ivan V. Fedyanin,[b,c] Alla N. Pivkina,[d] Dmitry B. Meerov,[d] Tatiana S. Kon'kova,[d] Yurii N. Matyushin,[d] Yurii A. Strelenko,[a] Kirill S. Erokhin,[a] Victor P. Zelenov[a] and Vladimir A. Tartakovsky[a]

[a] *N. D. Zelinsky Institute of Organic Chemistry, Russian Academy of Sciences, 47 Leninsky prosp., Moscow, 119991, Russian Federation. E-mail: voronin@ioc.ac.ru*
[b] *A. N. Nesmeyanov Institute of Organoelement Compounds, Russian Academy of Sciences, 28 Vavilova St., Moscow, 119991, Russian Federation*
[c] *HSE University, 101000 Moscow, Russian Federatio*
[d] *N.N. Semenov Federal Research Center for Chemical Physics, Russian Academy of Sciences, 4 Kosygina St., Building 1, 119991, Moscow, Russian Federation*

e-mails: voronin@ioc.ac.ru, churakov@ioc.ac.ru, a.churakov@mail.ru,

Contents

Experimental section

CAUTION!!! Although we have encountered no difficulties during preparation and handling of the compounds described in this paper, they are potentially explosive energetic materials that are sensitive to impact and friction. Any manipulations must be carried out by using appropriate standard safety precautions.

General remarks. All reactions were carried out in well-cleaned oven-dried glassware with magnetic stirring. ^{1}H, ^{13}C, ^{14}N spectra were recorded with Bruker DRX-500 (500.1, 125.8, 36.1 MHz) and Bruker AV600 (600.1, 150.9, 43.4) spectrometers. Chemical shifts are reported in delta (δ) units, parts per million (ppm) downfield from internal TMS (^{1}H, ^{13}C) or external CH_3NO_2 (^{14}N negative values of δ_N correspond to upfield shifts); multiplicities are indicated by s (singlet), d (doublet), t (triplet), q (quartet), m (multiplet) and br (broad). IR spectra were recorded with a Bruker "ALPHA-T" spectrometer in the range 400–4000 cm^{-1} (resolution 2 cm^{-1}) as pellets with KBr. Elemental analyses were performed by the CHNSO Analyzer Leco TruSpec Micro. Analytical thin-layer chromatography (TLC) was carried out on Merck 25 TLC silica gel 60 F254 aluminum sheets. The visualization of the TLC plates was accomplished with a UV light. Silica gel 60 Merck (15–40 μm) was used for preparative column chromatography. All reagents were purchased from Acros or Sigma–Aldrich. Solvents were purified before use, according to standard procedures. Ammonium and hydrazinium salts of 4*H*-[1,2,3]triazolo[4,5-c][1,2,5]oxadiazole 5-oxide **3b** and **3c** were prepared according to previously published procedure.[1]

[1] A. A. Voronin, I. V. Fedyanin, A. M. Churakov, A. N. Pivkina, N. V. Muravyev, Y. A. Strelenko, M. S. Klenov, D. B. Lempert and V. A. Tartakovsky, 4*H*-[1,2,3]Triazolo[4,5-*c*][1,2,5]oxadiazole 5-oxide and Its Salts: Promising Multipurpose Energetic Materials, *ACS Appl. Energ. Mat.*, 2020, **3**(9), 9401–9407. https://doi.org/10.1021/acsaem.0c01769

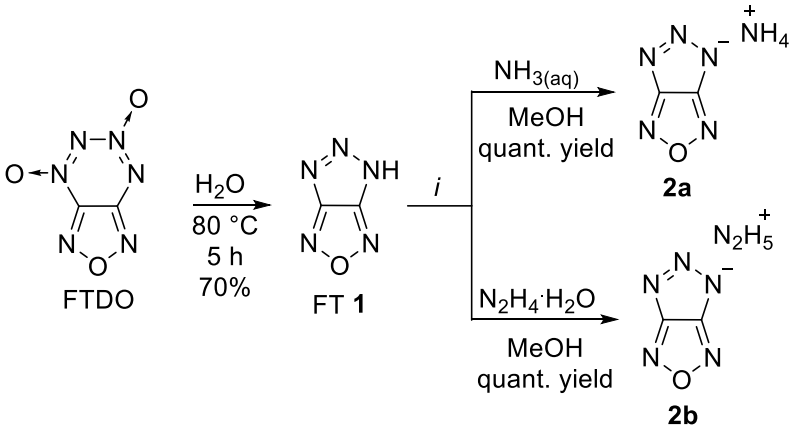

i: 1) FTDO trace extraction with PhH; 2) TF **1** extraction with Et_2O and subsequent evaporation of Et_2O

4*H*-[1,2,3]triazolo[4,5-*c*][1,2,5]oxadiazole (1).

A suspension of FTDO (4.5 g, 29 mmol) in distilled H_2O (400 mL) was heated to 80 °C (FTDO fully dissolved in H_2O) and stirred for 5 h at this temperature, then it was cooled to rt. Unreacted FTDO was extracted with benzene (2□200 mL), water phase was extracted with Et_2O (2□200 mL). Ether solution was dried ($MgSO_4$) and solvent was evaporated *in vacuo* to give viscous oil slowly crystalizing into from slightly colored to yellow solid (the color mainly depends on quality of starting FTDO) good enough for further use. If it is required product **1** can be purified by column chromatography (ethyl acetate). Compound **1** (2.3 g, 70%) obtained was identical to that described earlier[2]. Benzene solution was dried ($MgSO_4$) and solvent was evaporated *in vacuo* to give bright yellow oil (0.5 g) consisting mainly of FTDO, which can be stored for approximately 1 week in freezer and can be reused for hydrolysis.

^{1}H NMR (600.1 MHz, [D_6]-DMSO): δ 14.52 (br.s., 1 H, N**H**)

^{13}C NMR (150.9 MHz, [D_6]-DMSO): δ 163.0 (C-3a and C-6a)) ppm.

^{14}N NMR (43.4 MHz, [D_6]-acetone): 43, 13 (br.s., N-1 and N-3 and N-5), –116 (**N**H, $\nu_{½}$ = 310 Hz).

Elemental analysis calcd (%) for $C_2H_1N_5O_1$: C 21.63, H 0.91, N 63.06; found C 21.89, H 1.12, N 62.47.

[2] V. P.Zelenov, A. A.Lobanova, N. I. Lyukshenko, S. V. Sysolyatin and A. I. Kalashnikov A.I. Behavior of [1,2,5]oxadiazolo[3,4-*e*][1,2,3,4]tetrazine 4,6-dioxide in various media, *Russ. Chem. Bull.*, 2008, **57**(7), 1384–1389. https://doi.org/10.1007/s11172-008-0180-y

General procedure for the preparation of the ammonium (2a) and hydrazinium (2b) salts

To a vigorously stirred solution of H-form **1** (10 mmol) in MeOH (30 mL) an equimolar amount of 25% ammonia solution (in case of **2b**) or $NH_2NH_2 \cdot H_2O$ (in case of **2c**) was added dropwise at room temperature. After 30 min stirring, the solvent was evaporated *in vacuo* and the residue was recrystallized from MeCN.

Ammonium salt of 4*H*-[1,2,3]triazolo[4,5-*c*][1,2,5]oxadiazole (2a):

Quantitative yield; yellow solid;

^{1}H NMR (600.1 MHz, [D_6]-DMSO): δ 7.23 (br.s., 4 H, N**H**$_4$)

^{13}C NMR (150.9 MHz, [D_6]-DMSO): δ 170.7 (C-3a and C-6a)) ppm.

^{14}N NMR (43.4 MHz, [D_6]-DMSO): 94 (N-5, $\nu_{½}$ = 400 Hz), 2 (N-1 and N-3, $\nu_{½}$ = 450 Hz), –78 (N-4 and N-6, $\nu_{½}$ = 240 Hz), –358 (**N**H$_4$, $\nu_{½}$ = 6 Hz)

IR (KBr): $\tilde{\nu}$ 509, 556, 664, 715, 775, 807, 827, 994, 1048, 1278, 1407, 1436, 1451, 1492, 1866, 2075, 2120, 2151, 2804, 2972, 3099, 3209 cm^{-1}.

Elemental analysis calcd (%) for $C_2H_4N_6O_1$: C 18.75, H 3.15, N 65.61; found C 18.63, H 3.14, N 63.92.

Hydrazinium salt of 4*H*-[1,2,3]triazolo[4,5-*c*][1,2,5]oxadiazole (2b):

Quantitative yield; lemon-colored solid;

^{1}H NMR (500.1 MHz, [D_6]-DMSO): δ 6.82 (br.s., 5 H, N_2**H**$_5$)

^{13}C NMR (125.8 MHz, [D_6]-DMSO): δ 170.8 (C-3a and C-6a)) ppm.

^{14}N NMR (36.1 MHz, [D_6]-DMSO): 95 (N-5, $\nu_{½}$ = 600 Hz), 3 (N-1 and N-3, $\nu_{½}$ = 460 Hz), –78 (N-4 and N-6, $\nu_{½}$ = 285 Hz), –333 (**N**$_2$H$_5$, $\nu_{½}$ = 850 Hz)

IR (KBr): $\tilde{\nu}$ 500, 560, 573, 719, 798, 826, 956, 971, 1035, 1063, 1105, 1137, 1150, 1281, 1419, 1444, 1527, 1604, 2044, 2101, 2127, 2648, 2719, 2859, 2961, 3085, 3157, 3249, 3323 cm^{-1}.

Elemental analysis calcd (%) for $C_2H_5N_7O_1$: C 16.79, H 3.52, N 68.51; found C 16.54, H 3.39, N 66.43.

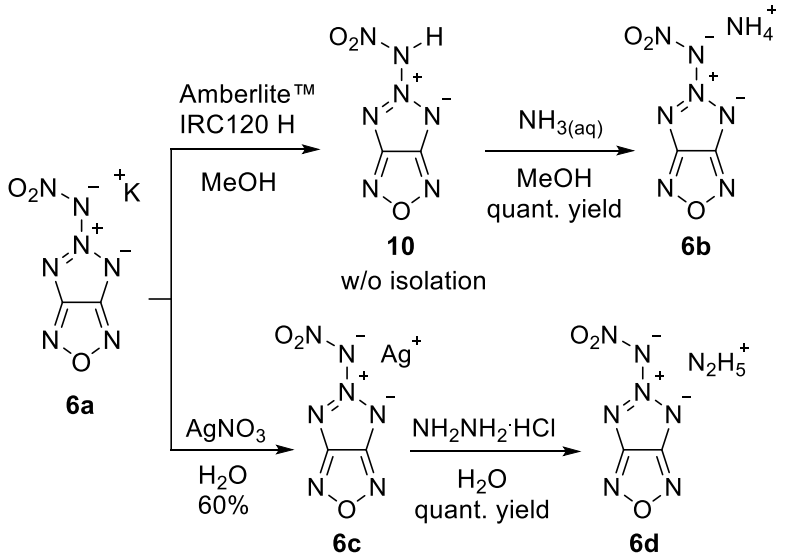

Ammonium salt of 5-(nitroamino)-[1,2,3]triazolo[4,5-*c*][1,2,5]oxadiazol-5-ium-4-ide (6b).

To a solution of K-salt **6a** (1.05 g, 5 mmol) in MeOH (15 mL) ion-exchange resin (Amberlite IR 120, H-form, 3 g) was added and the mixture was vigorously stirred for 1 h at room temperature. The ion-exchange resin was filtered off and the solution was neutralized with 25% ammonia solution in water to pH = 9–10 (indicator paper), then reaction mixture was stirred for 30 min, the solvent was evaporated *in vacuo*. Small amount of Et_2O (15 mL) was added to the residue and then evaporated *in vacuo*. This procedure triggered the crystallization of the ammonium salt **6b** obtained in quantitative yield (930 mg) as slightly yellow crystals. Extra pure salt was obtained by recrystallization from MeCN as the colors of melted milk crystals.

^{1}H NMR (600.1 MHz, [D_6]-DMSO): δ 7.07 (t, 4 H, N**H**$_4$, J = 50.6 Hz)

^{13}C NMR (150.9 MHz, [D_6]-DMSO): δ 163.1 (C-3a and C-6a)) ppm.

^{14}N NMR (43.4 MHz, [D_6]-DMSO): 20 (N-1 and N-3, br. s), –9 (**N**O_2, $\nu_{½}$ = 40 Hz), –48 (N-5, $\nu_{½}$ = 160 Hz), –90 (N-4 and N-6, $\nu_{½}$ = 1000 Hz), –359 (m, **N**H_4, J = 50.6 Hz)

IR (KBr): $\tilde{\nu}$ 426, 657, 751, 807, 828, 1027, 1054, 1178, 1229, 1309, 1402, 3168, 3318 cm^{-1}.

Elemental analysis calcd (%) for $C_2H_4N_8O_3$: C 12.77, H 2.14, N 59.57; found C 12.70, H 2.06, N 56.9.

Ag-Salt of 5-(nitroamino)-[1,2,3]triazolo[4,5-*c*][1,2,5]oxadiazol-5-ium-4-ide (6c).

Caution! Ag-Salt is very sensitive to impact and friction and has to be handled as a primary explosive. To a vigorously stirred solution of K-salt **6a** (627 mg, 3 mmol) in H_2O (10 mL), $AgNO_3$ (740 mg, 4.5 mmol) was added at 25 °C. The reaction mixture was stirred at 25 °C for 30 min and the precipitate was collected using porous metal filter, washed with H_2O (2×5 mL) and minimum

amount of cold MeOH, then dried under reduced pressure. Ag-Salt **6c** was obtained in the yield of 500 mg (60%); beige colored crystals. T_{dec} = 100–105 °C.

^{13}C NMR (125.8 MHz, [D_6]-DMSO): δ 163.0 (C-3a and C-6a)) ppm.

^{14}N NMR (36.1 MHz, [D_6]-DMSO): δ –9 (NO_2, $\nu_{½}$ = 45 Hz), –48 (N-5, $\nu_{½}$ = 190 Hz).

Hydrazinium salt of 5-(nitroamino)-[1,2,3]triazolo[4,5-*c*][1,2,5]oxadiazol-5-ium-4-ide (6d). To a vigorously stirred suspension of Ag-salt **6c** (420 mg, 1.5 mmol) in H_2O (10 mL) a hydrazinium monochloride (100 mg, 1.49 mmol) was added at room temperature. The resulting mixture was stirred at ambient temperature for 5 h. Then, AgCl was removed by filtration and the solvent was evaporated *in vacuo*. A small amount of MeCN (5 mL) was added to the residue and then evaporated *in vacuo* to trigger the crystallization of the hydrazinium salt **6d** obtained in quantitative yield (300 mg) as slightly yellow crystals. A sampler of pure salt **6d** was obtained by column chromatography (ethyl acetate).

^{13}C NMR (125.8 MHz, [D_4]-methanol): δ 164.7 (C(3a,6a)) ppm.

^{14}N NMR (36.1 MHz, [D_4]-methanol): 25 (N-1 and N-3, $\nu_{½}$ = 1000 Hz), –8 (**N**O_2, $\nu_{½}$ = 25 Hz), –53 (N-5, $\nu_{½}$ = 125 Hz), –88 (N-4 and N-6, $\nu_{½}$ = 600 Hz), –335(**N**$_2H_5$, $\nu_{½}$ = 510 Hz)

IR (KBr): $\tilde{\nu}$ 769, 811, 835, 960, 1053, 1088, 1105, 1128, 1193, 1227, 1308, 1429, 1611, 2146, 3067, 3168, 3275, 3316 cm^{-1}.

Elemental analysis calcd (%) for $C_2H_5N_9O_3$: C 12.00, H 2.37, N 59.97; found C 11.83, H 2.48, N 62.06.

NMR and IR section

^{1}H NMR spectrum of salt 2a (NH_4TF) in DMSO-d_6

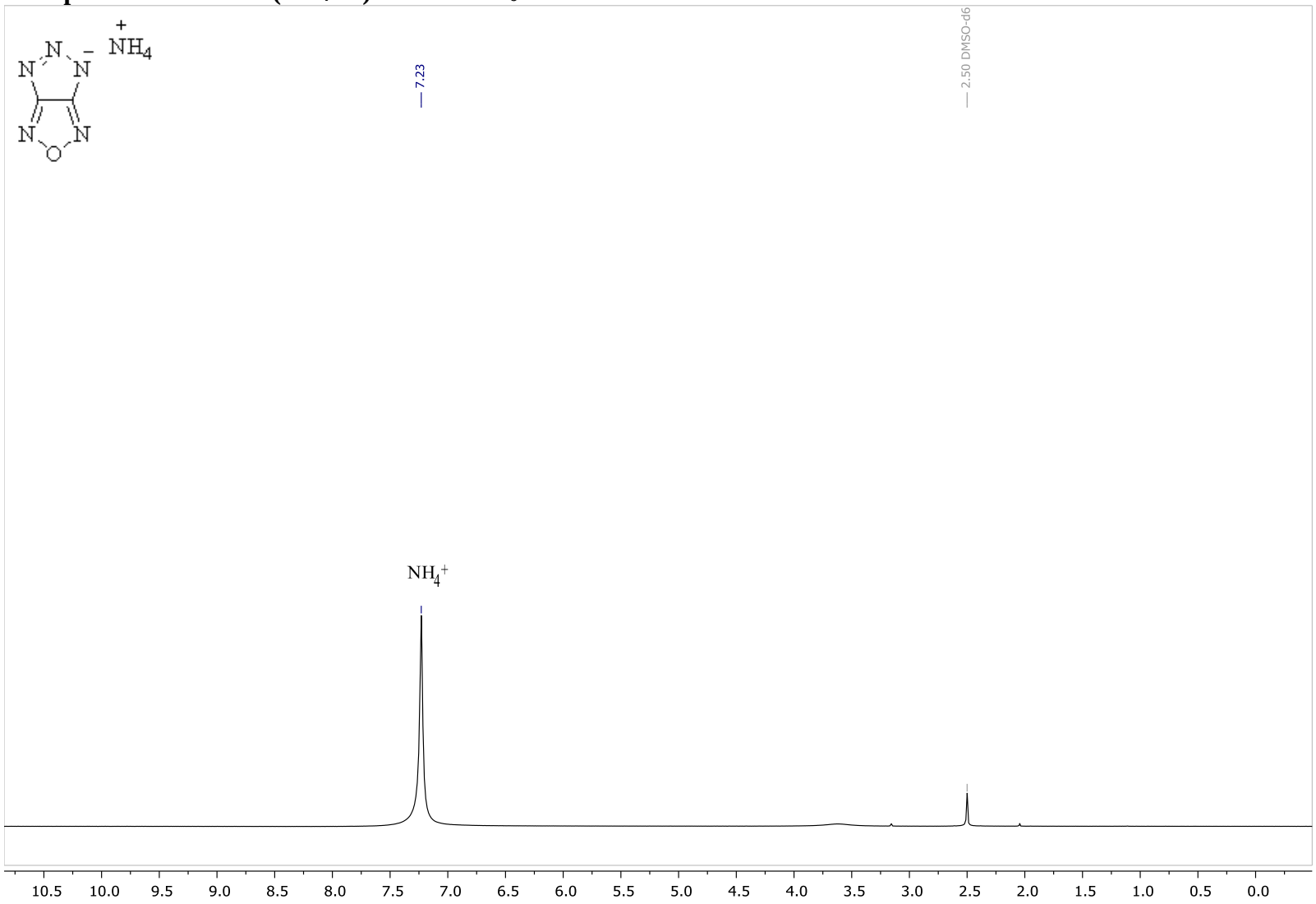

^{13}C NMR spectrum of salt 2a (NH_4TF) in DMSO-d_6

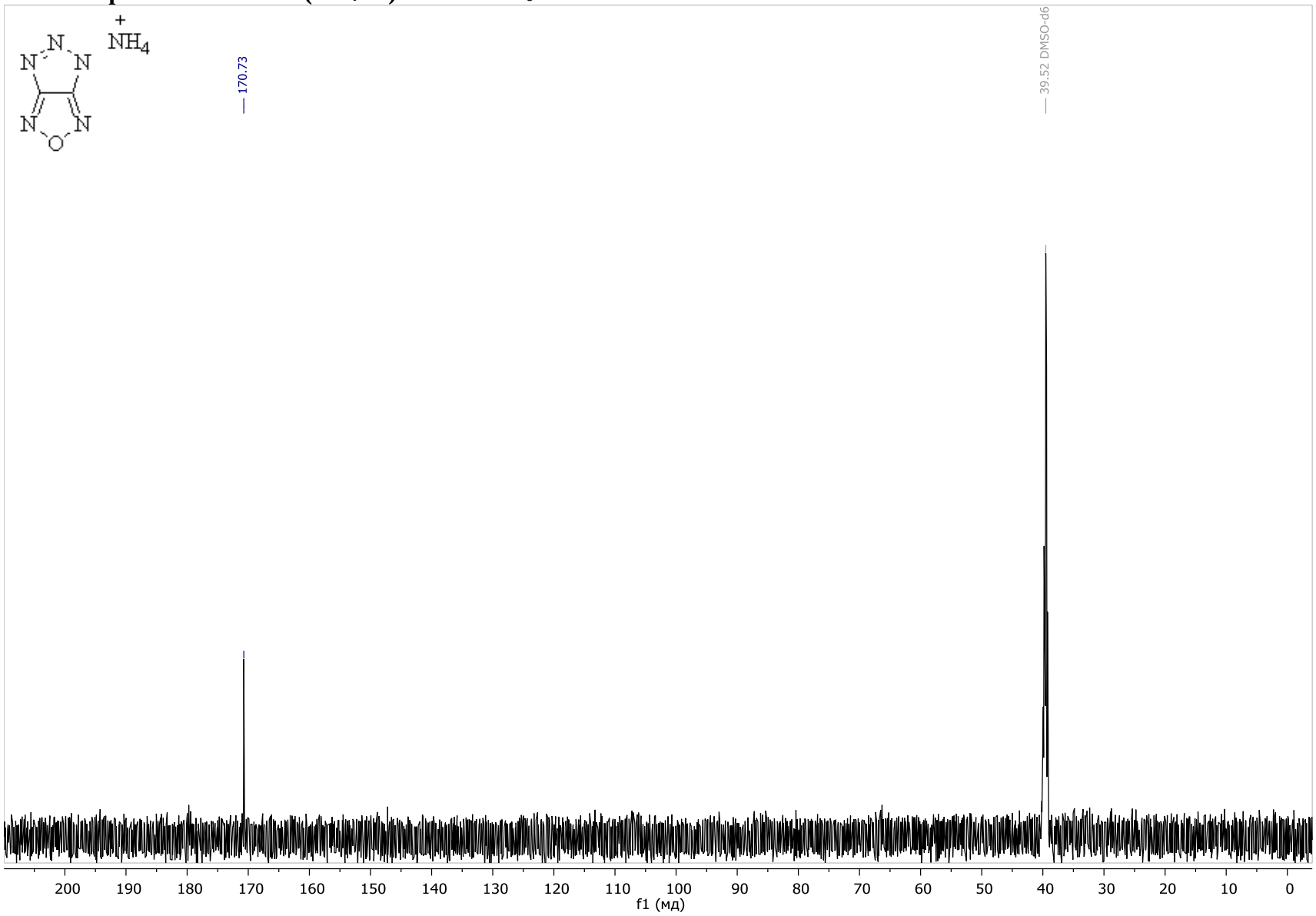

^{14}N NMR spectrum of salt 2a (NH_4TF) in DMSO-d_6

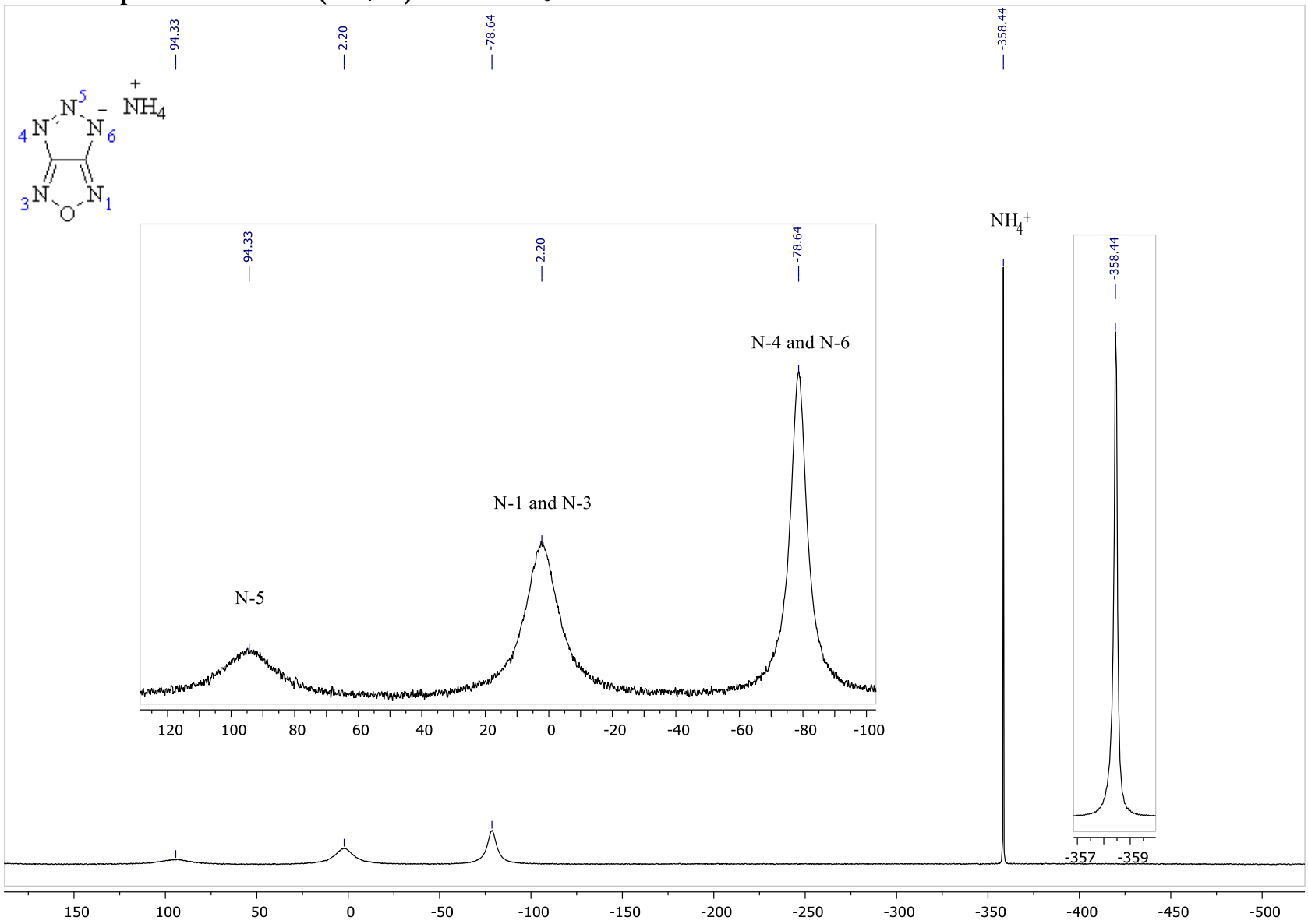

IR (KBr) spectrum of salt 2a (NH_4TF)

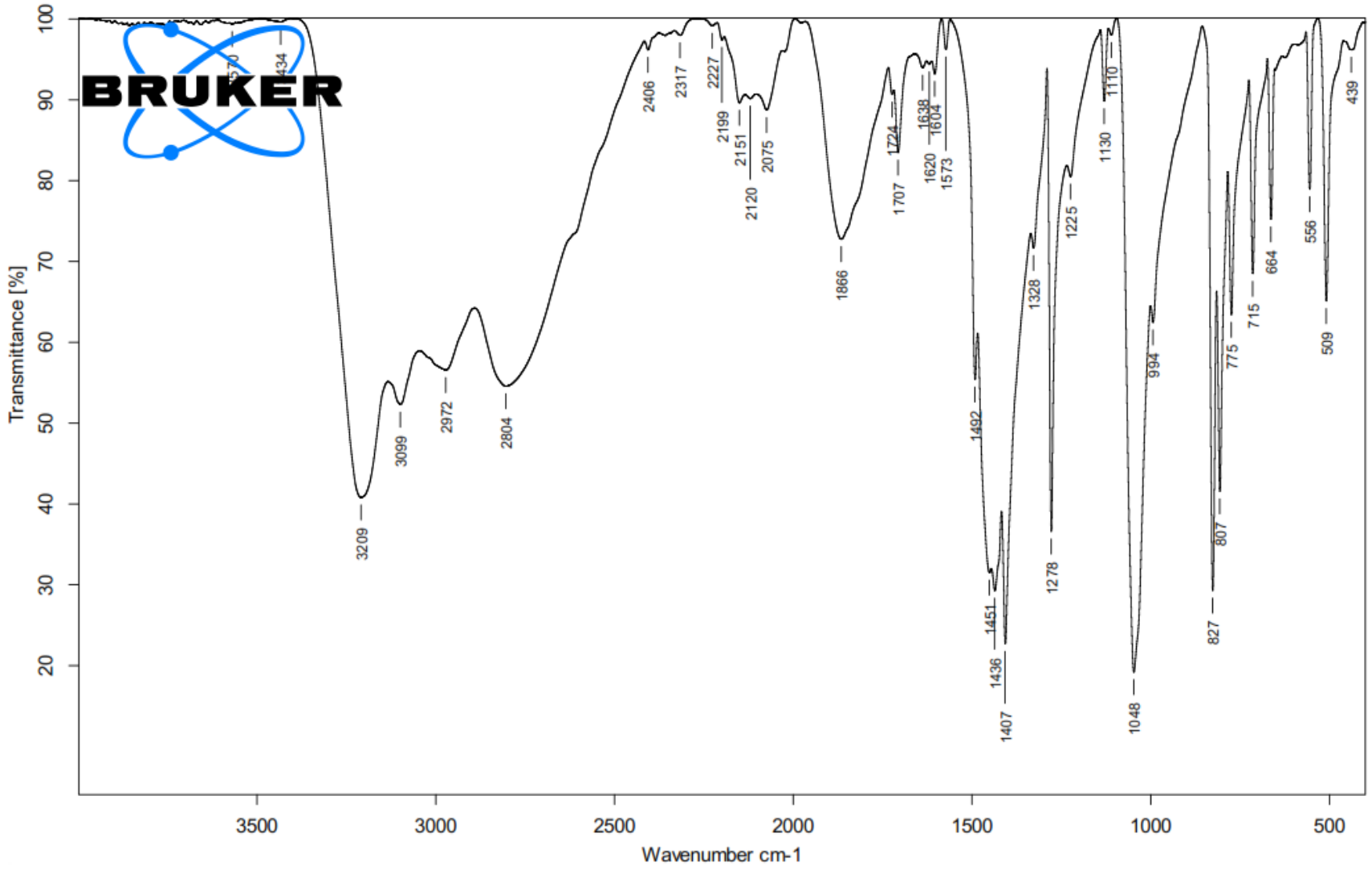

^{1}H NMR spectrum of salt 2b (N_2H_5TF) in DMSO-d_6

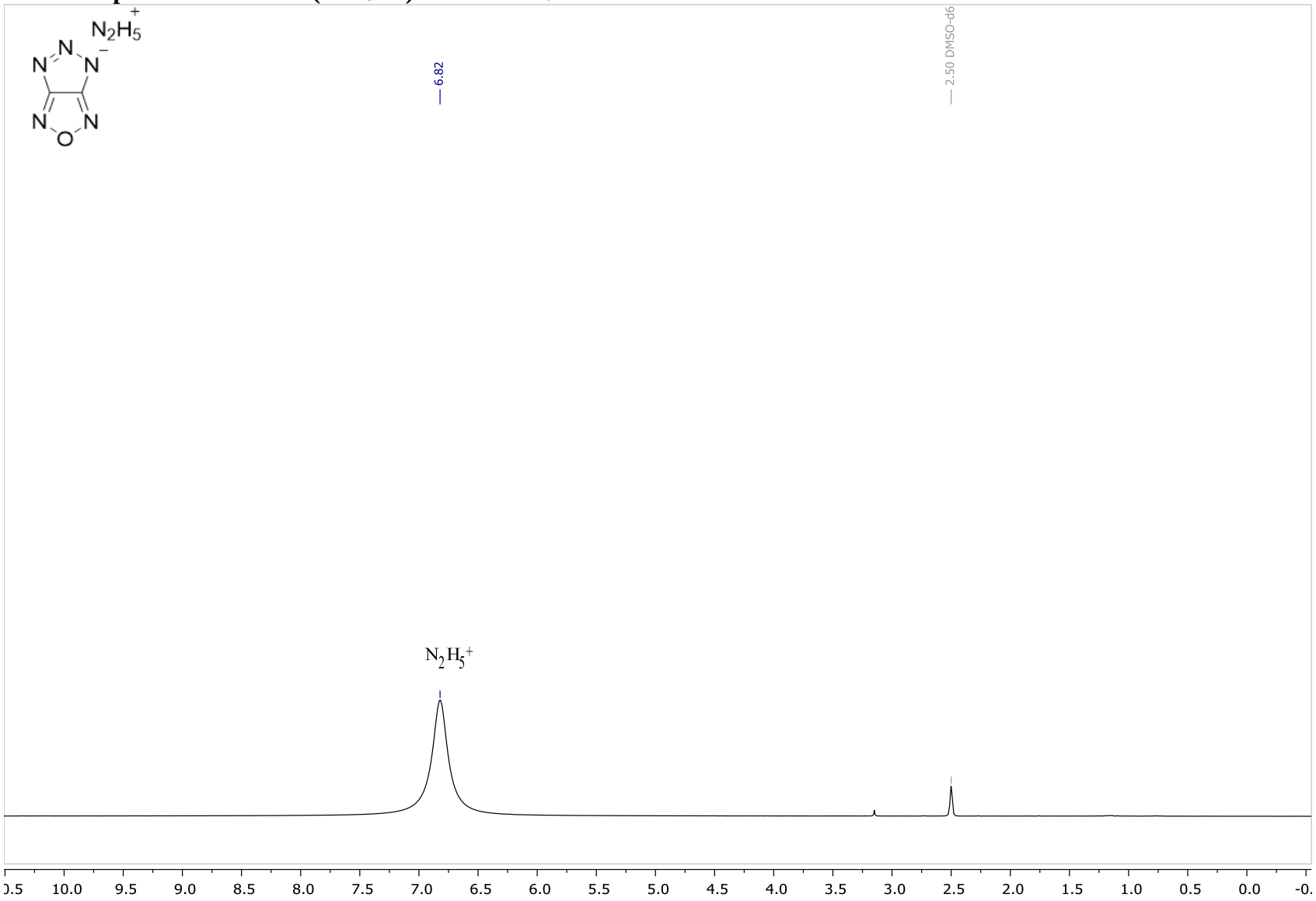

^{13}C NMR spectrum of 2b (N_2H_5TF) in DMSO-d_6

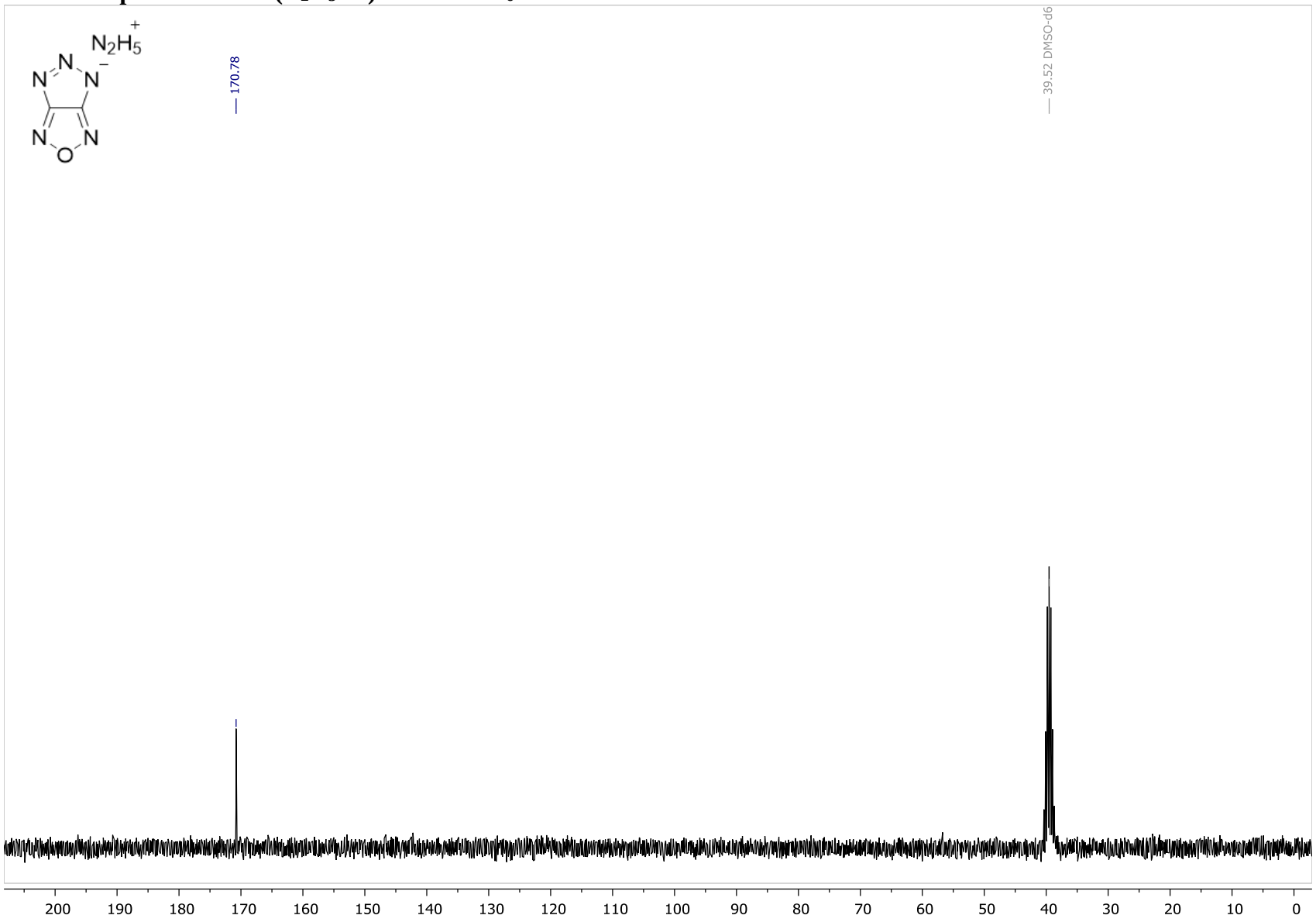

^{14}N NMR spectrum of 2b (N_2H_5TF) in DMSO-d_6

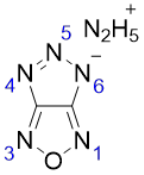

IR (KBr) spectrum of salt 2b (N_2H_5TF)

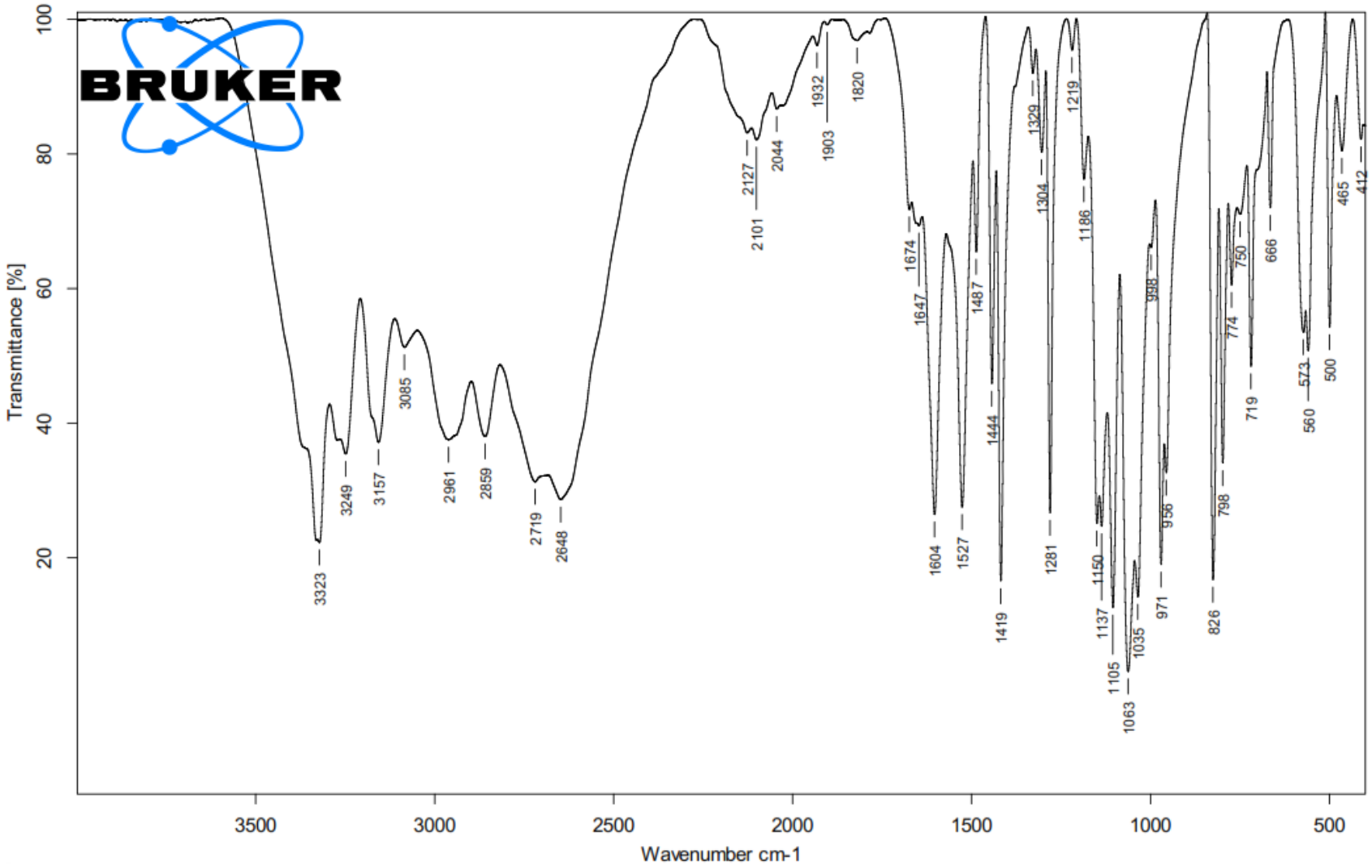

^{1}H NMR spectrum of salt 6b (NH_4TFNA) in DMSO-d_6

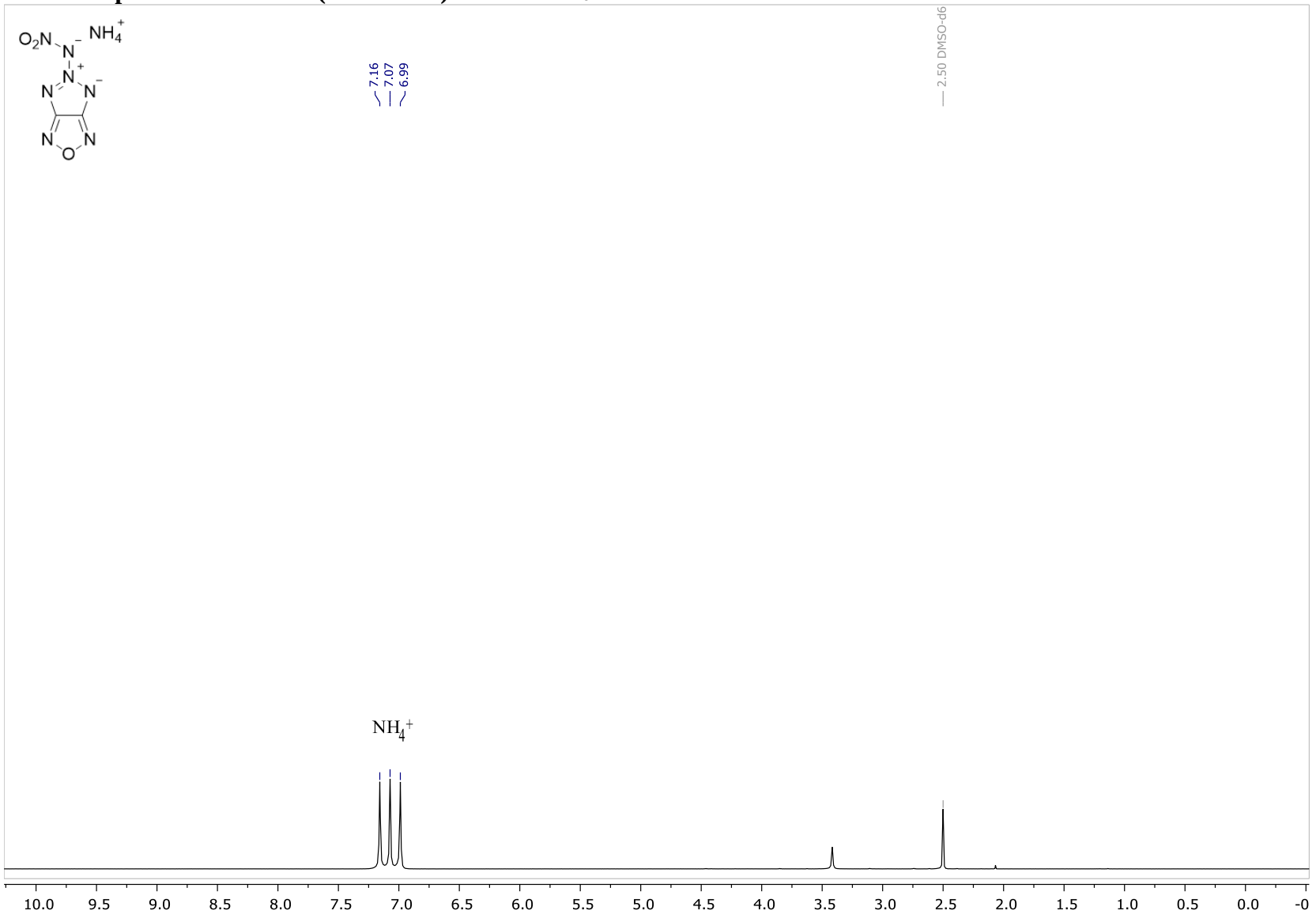

^{13}C NMR spectrum of salt 6b (NH_4TFNA) in DMSO-d_6

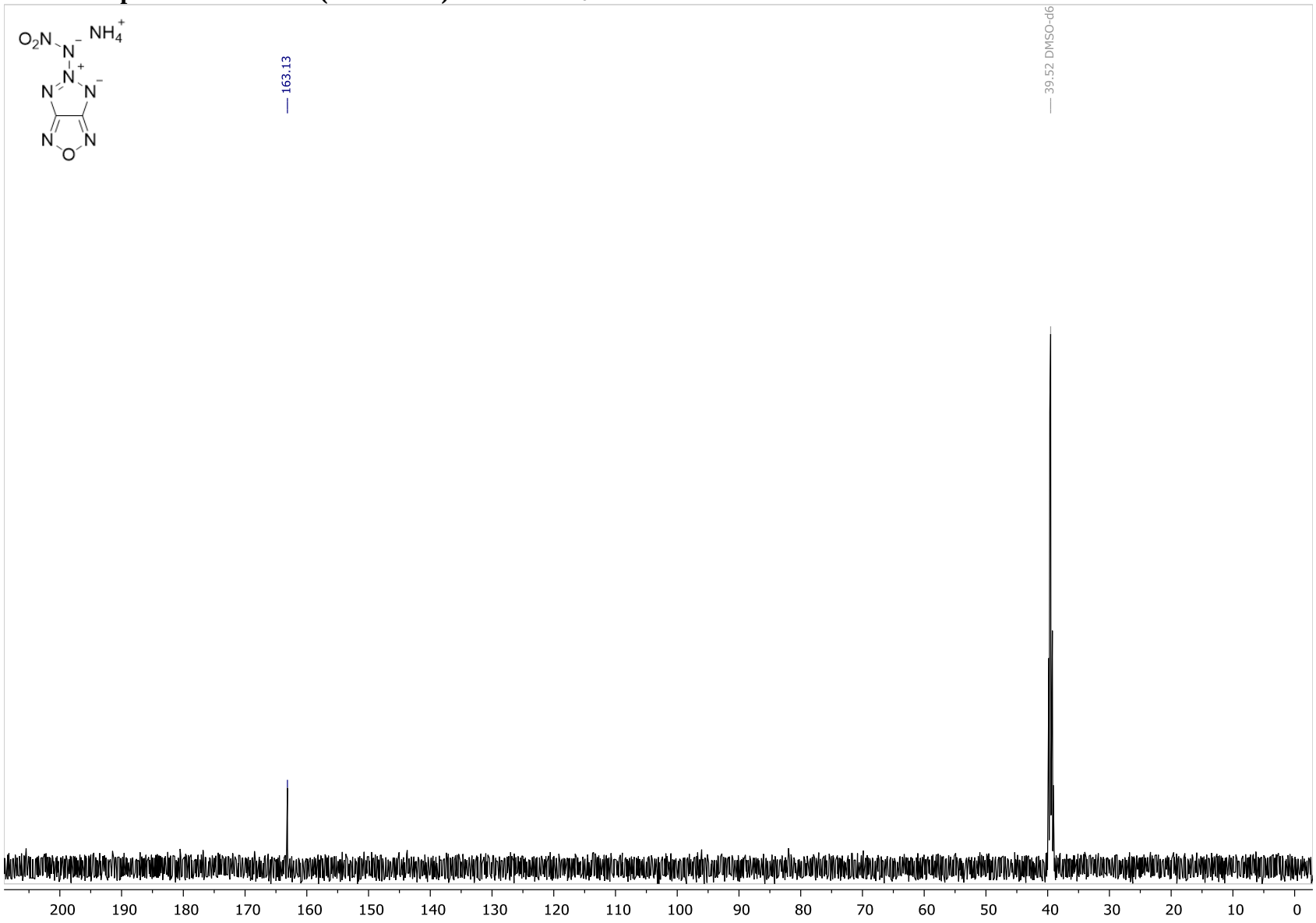

^{14}N NMR spectrum of salt 6b (NH_4TFNA) in DMSO-d_6

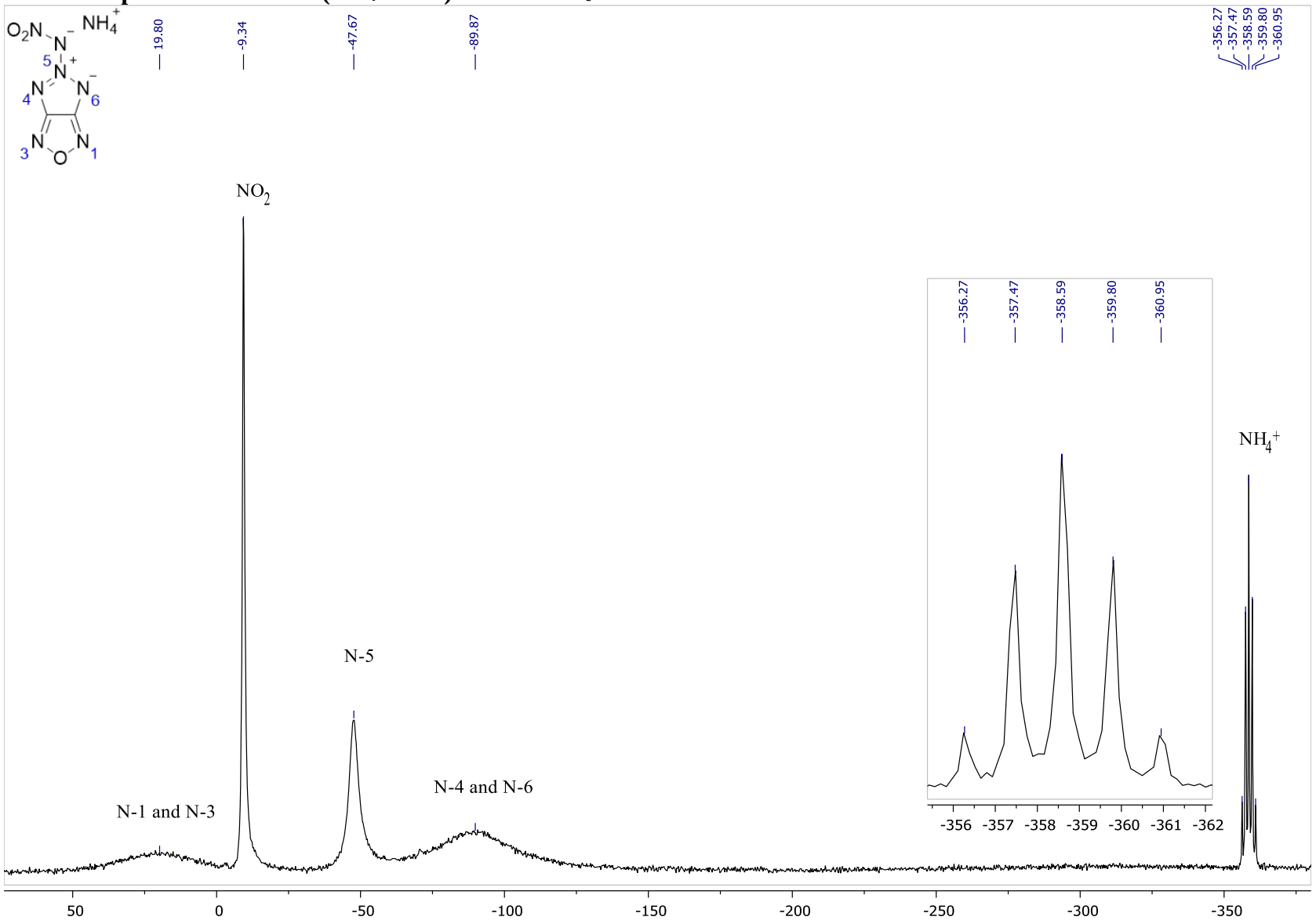

IR (KBr) spectrum of salt 6b (NH_4TFNA)

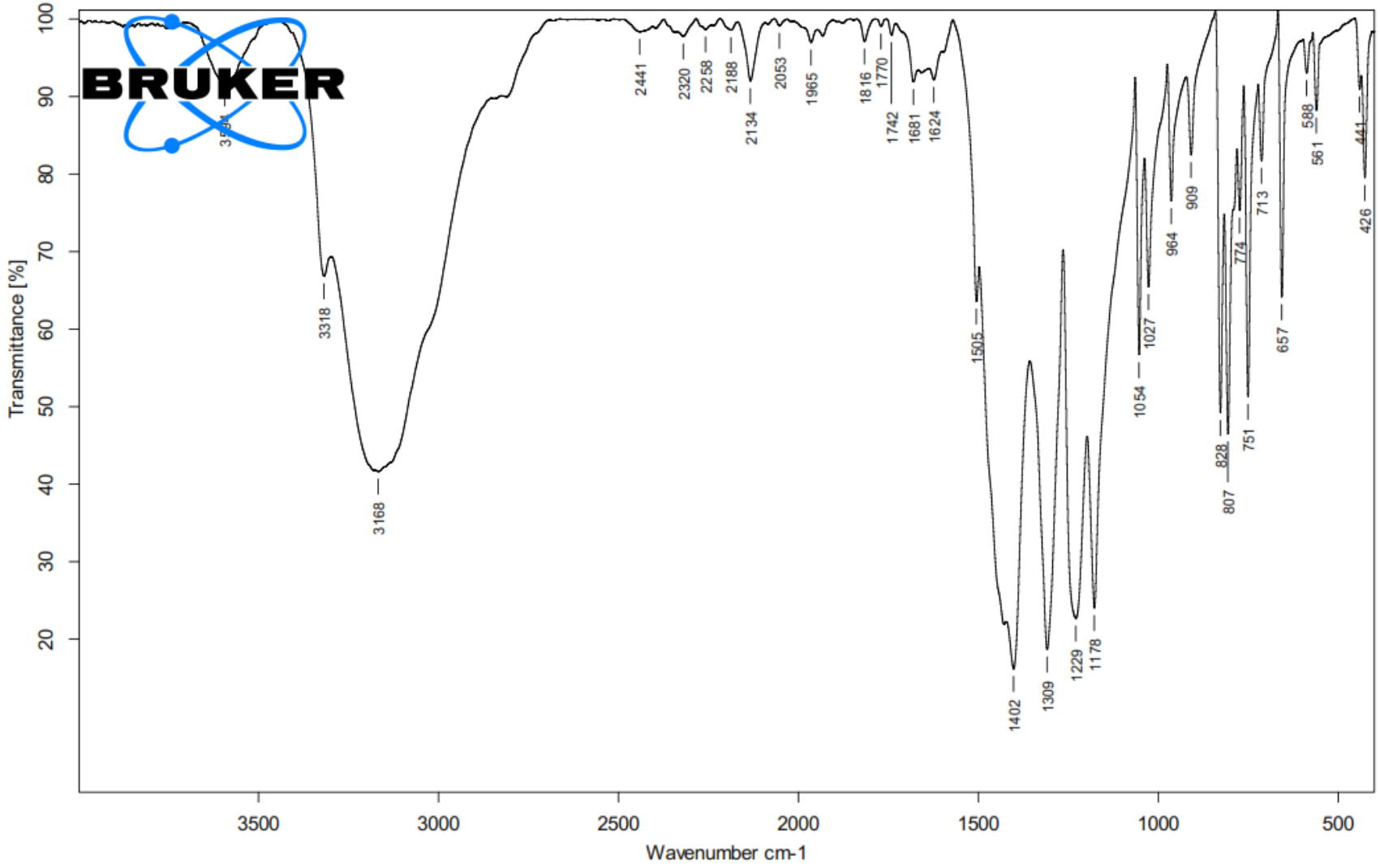

^{13}C NMR spectrum for salt 6c (AgTFNA) in DMSO-d$_6$

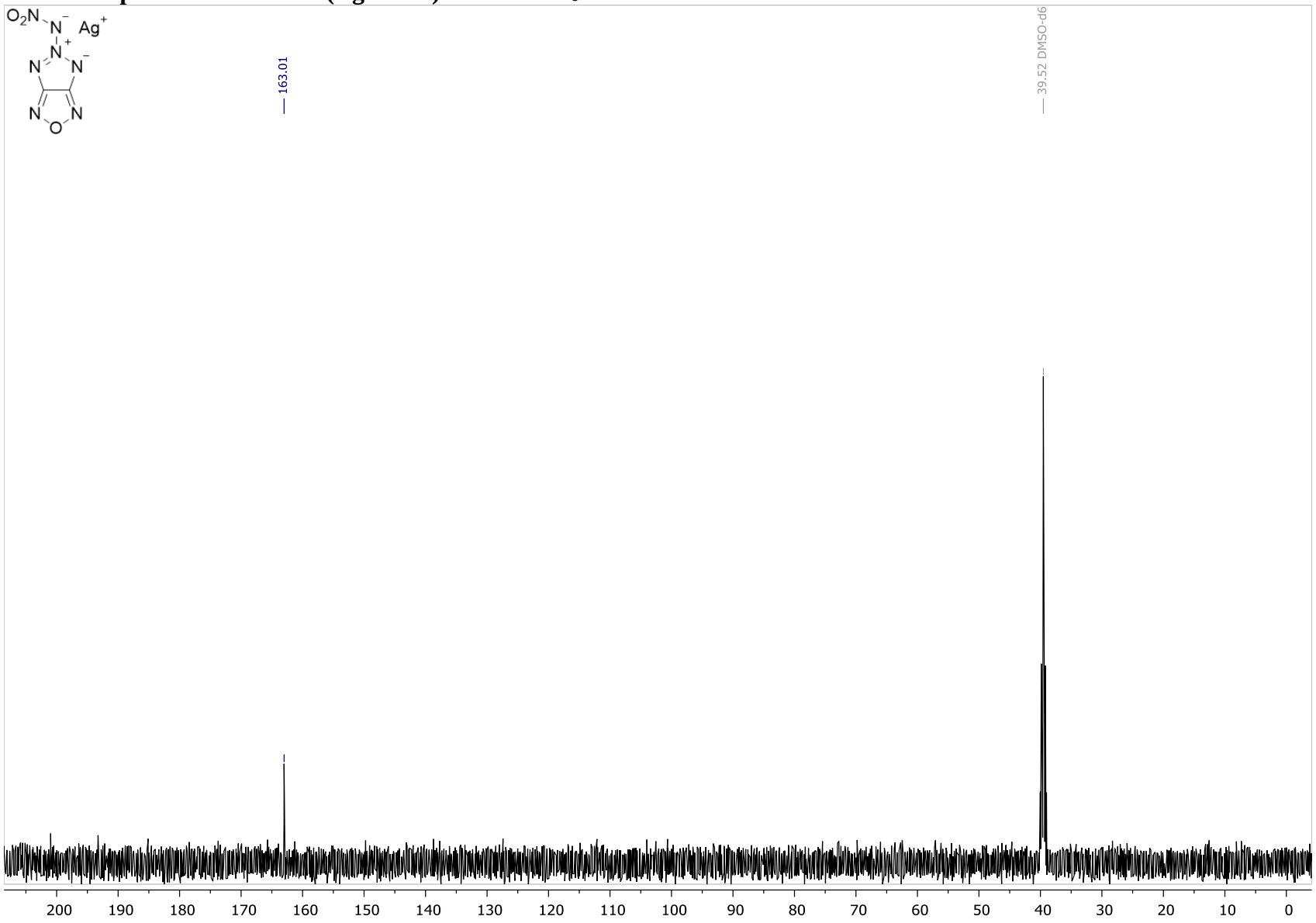

^{14}N NMR spectrum for salt 6c (AgTFNA) in DMSO-d$_6$

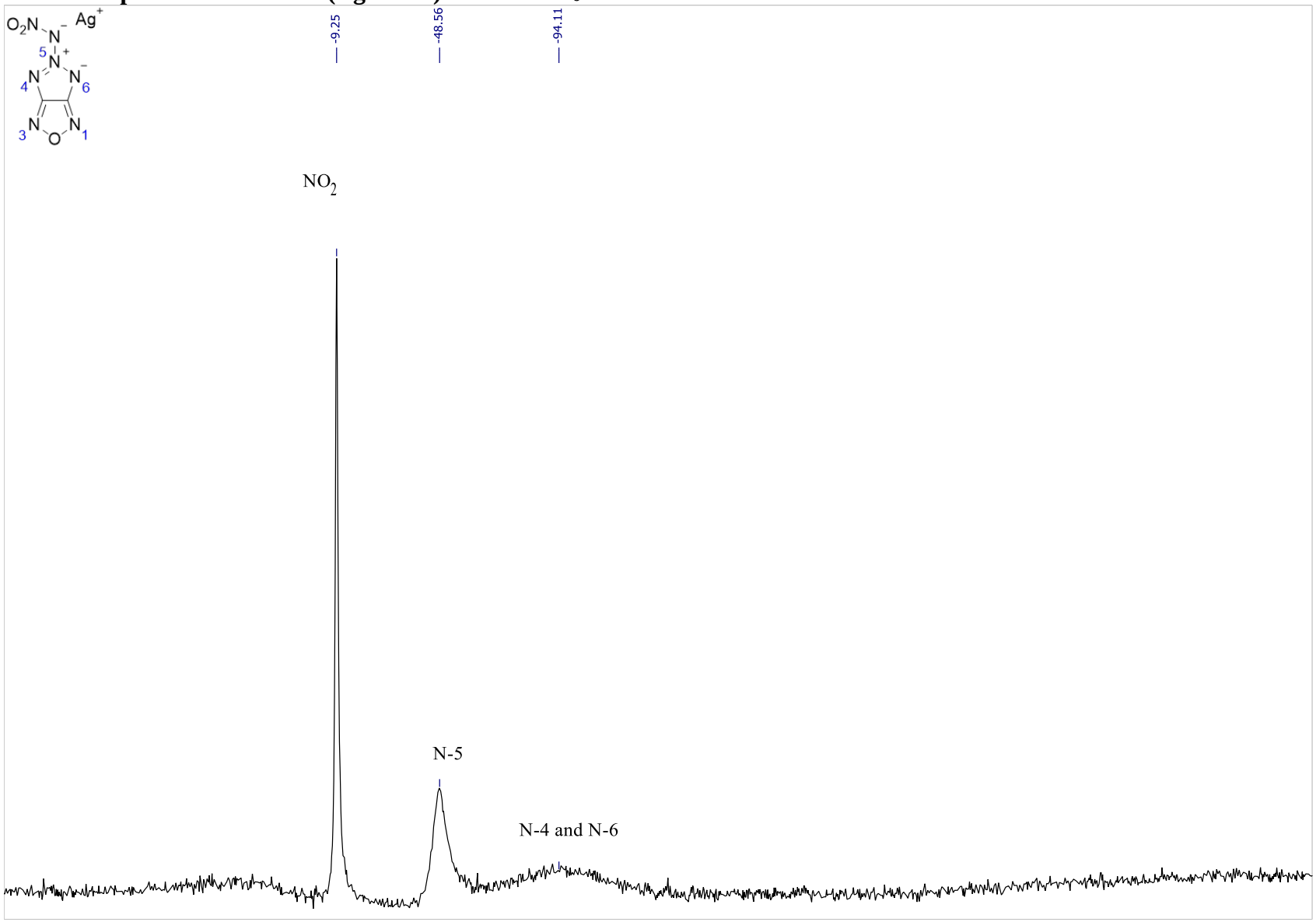

^{13}C NMR spectrum for salt 6d (N_2H_5TFNA) in methanol-d_4

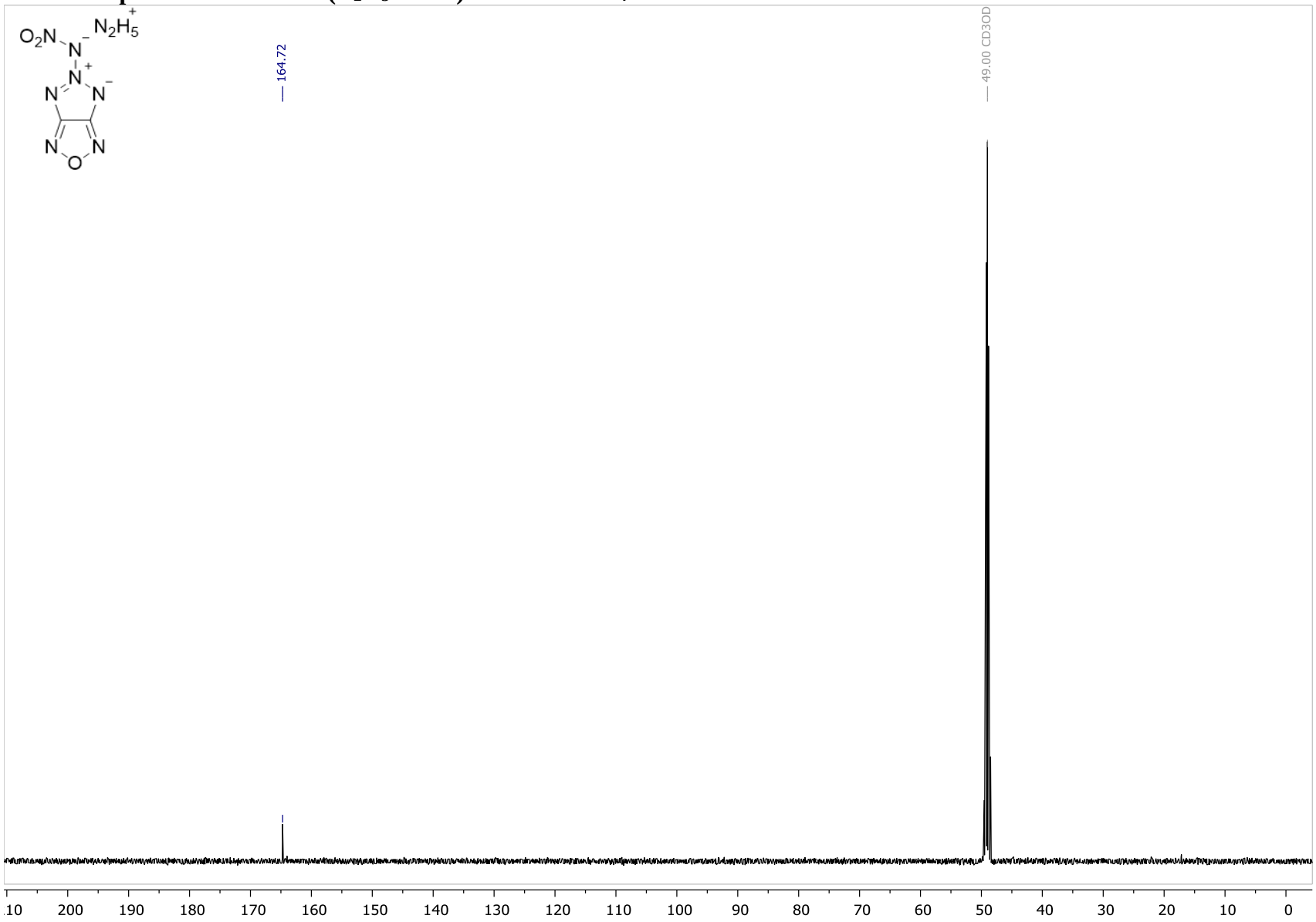

^{14}N NMR spectrum for salt 6d (N_2H_5TFNA) in methanol-d_4

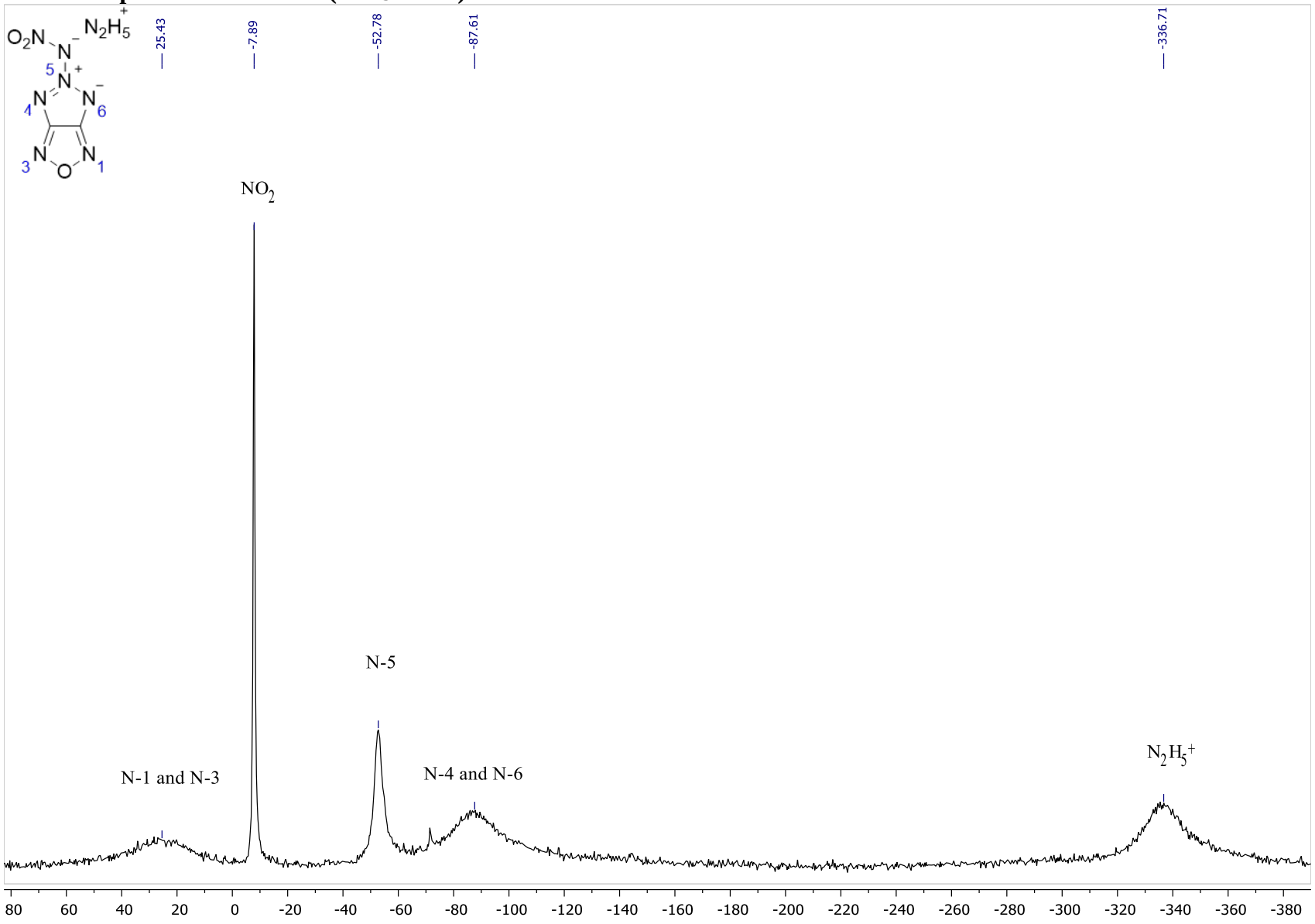

IR spectrum for salt 6d (N_2H_5TFNA)

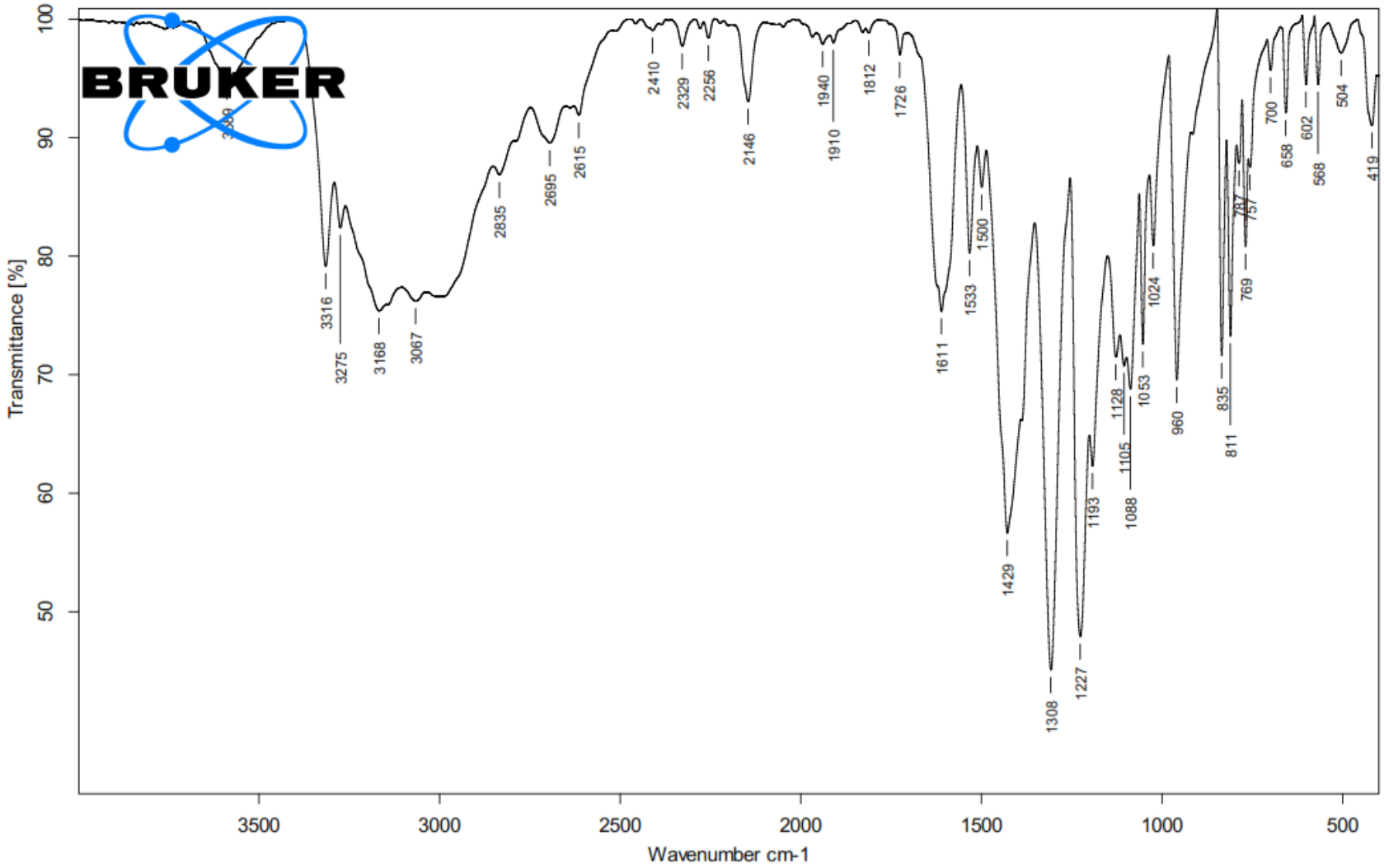

X-ray crystallographic section

Computation details

Ab initio calculations were performed with the ORCA software package, version 5.0.3.[3] Full geometry optimization of anions **2**, **3** and **6** and the corresponding H-forms **1**, **5**, and **10** was performed with the density functional theory (DFT) approach with the PBE0-D3(BJ)[4,5] functional and def2-TZVPP basis set[6]. Harmonic frequencies were calculated to account for zero-point vibration energy. Nucleus independent chemical shifts ($NICS(1)_{zz}$) were calculated by the GIAO method, as the negative of the zz components of the shielding tensors in dummy points 1 Å above the ring centers.[7]

Experimental

Single crystal X-ray diffraction experiments were performed on a Bruker Quest diffractometer equipped with PHOTON 3 detector and operating with graphite-monochromated MoKα (λ = 0.71073 Å). Frames were integrated using the Bruker SAINT[8] software package by a narrow-frame algorithm. A semi-empirical absorption correction was applied with the SADABS program[9] using the intensity data of equivalent reflections. The structures were solved with the dual-space method with SHELXT program[10] and refined by the full-matrix least-squares technique against F^2_{hkl} in anisotropic approximation with SHELXL program[11]. Hydrogen atoms were found from difference Fourier synthesis and refined in isotropic approximation.

---

[3] F. Neese, Software update: The ORCA program system — Version 5.0, *WIREs Comput. Mol. Sci.*, 2022, **12**, e1606. https://doi.org10.1002/wcms.1606

[4] C. Adamo and V. Barone, Toward reliable density functional methods without adjustable parameters: The PBE0 model, *J. Chem. Phys.* 1999, **110**(13), 6158–6170. https://doi.org/10.1063/1.478522

[5] S. Grimme, S. Ehrlich and L. Goerigk, Effect of the damping function in dispersion corrected density functional theory, *J. Comput. Chem.* 2011, **32**(7), 1456–1465. https://doi.org/10.1002/jcc.21759

[6] M. F. Peintinger, D. V. Oliveira and T. Bredow, Consistent Gaussian basis sets of triple-zeta valence with polarization quality for solid-state calculations *J. Comput. Chem.* 2013, **34**(6), 451–459. https://doi.org/10.1002/jcc.23153

[7] K. Wolinski, J. F. Hinton and P. Pulay, Efficient implementation of the gauge-independent atomic orbital method for NMR chemical shift calculations, *J. Am. Chem. Soc.*, 1990, **112**(23), 8251–8260. https://doi.org/10.1021/ja00179a005

[8] Bruker, SAINT v8.34A, 2013.

[9] L. Krause, R. Herbst-Irmer, G. M. Sheldrick and D. Stalke, Comparison of silver and molybdenum microfocus X-ray sources for single-crystal structure determination, *J. Appl. Crystallogr.*, 2015, **48**(1), 3–10. https://doi.org/10.1107/S1600576714022985

[10] G. M. Sheldrick, SHELXT – Integrated space-group and crystal-structure determination, *Acta Crystallogr. Sect. Found. Adv.*, 2015, **71**(1), 3–8. https://doi.org/10.1107/S2053273314026370

[11] G. M. Sheldrick, Crystal structure refinement with SHELXL, *Acta Crystallogr. Sect. C Struct. Chem.*, 2015, **71**(1), 3–8. https://doi.org/10.1107/S2053229614024218

X-ray powder diffraction studies were performed on a Bruker AXS D8 diffractometer equipped with a LynxEye position sensitive detector and operating CuKα radiation (λ = 1.534 Å) in reflection mode. Samples were placed on a zero-background silicon sample holder and rotated at a speed of 60 deg/min. Data collection was performed at ambient temperature with a step size of 0.01° for 2θ ranges of 3–60°. The diffraction patterns of the samples **6b-II** and **6d** were indexed using the SVD (singular value decomposition) indexing algorithm[12] as implemented in the Bruker TOPAS 5.0 software[13], and the space group was determined using the analysis of systematic absences. For the phase analysis, the constrained Rietveld refinement was performed with fixed atomic fractional coordinates taken from single-crystal experiments at 100 K, for the other salts the Pawley fit was used.

Crystallographic data for all structures were deposited with the Cambridge Crystallographic Data Centre, CCDC 2308527-2308529 and 2308531 are available free of charge via https://www.ccdc.cam.ac.uk/structures/.

Table SIF1. Crystallographic data for salts **2a,b, 2b·H_2O, 3b,c, 6b,d**

	2a	**2b**	**2b·H_2O**	**3b**[a]	**3c**[a]	**6b-I**	**6b-II**	**6d**
CCDC/ CSD	2308527	2308528	2308529	1992732/ ENAHUZ	1992736/ ENAJOV	2308531		
Formula	$C_2H_4N_6O$	$C_2H_5N_7O$	$C_2H_7N_7O_2$	$C_2H_4N_6O_2$	$C_2H_5N_7O_2$	$C_2H_4N_8O_3$	$C_2H_4N_8O_3$	$C_2H_5N_9O_3$
M, g cm^{-3}	128.11	143.13	161.15	144.11	159.13	188.13	188.13	203.15
T, K	100	100	100	120	120	100		
Crystal system	orthorhombic	orthorhombic	orthorhombic	monoclinic	monoclinic	monoclinic	monoclinic	orthorhombic
Sp. group	*Pmna*	*Pna*2$_1$	*Pca*2$_1$	*Pc*	*P*2$_1$	*C*2/*c*	*P*2$_1$/*c*	*P*2$_1$2$_1$2$_1$
Z / *Z*'	4 / 1	8 / 2	4 / 1	8 / 4	2 / 1	8 / 1	4 / 1	4 / 1
a, Å	12.1399(8)	14.1872(15)	19.6742(16)	9.9276(4)	3.6166(3)	20.0924(5)		
b, Å	3.6287(3)	9.3706(7)	3.7044(3)	13.3146(5)	9.2588(7)	5.83450(10)		
c, Å	11.6102(7)	8.6822(8)	8.6710(6)	9.7211(4)	9.2664(7)	12.1652(3)		
α, °								
β, °				118.924(2)	99.947(2)	98.8230(10)		
γ, °								
V, Å^3	511.45(6)	1154.23(18)	631.95(8)	1124.67(8)	305.62(4)	1409.24(6)		
d_{calc}, g·cm^{-3}	1.664	1.647	1.694	1.702	1.729	1.773		
μ, cm^{-1}	1.37	1.36	1.45	1.48	1.49	1.59		
$2\theta_{max}$, °	60	56	60			60		
Collected reflns.	4888	15195	6092			10779		

[12] A. A. Coelho, Indexing of powder diffraction patterns by iterative use of singular value decomposition, *J. Appl. Crystallogr.*, 2003, **36**, 86–95. https://doi.org/10.1107/S0021889802019878

[13] A. A. Coelho, TOPAS and TOPAS-Academic: an optimization program integrating computer algebra and crystallographic objects written in C++, *J. Appl. Crystallogr.*, 2018, **51**, 210–218. https://doi.org/10.1107/S1600576718000183

Independent reflns.	781	2779	1740			2023		
Reflns with. I>2s(I)	650	2122	1618			1893		
R_1	0.0441	0.0550	0.0399			0.0293		
wR_2	0.1116	0.1164	0.0960			0.0801		
GOF	1.028	1.009	1.051			1.074		
Residual density, e Å^{-3}	0.460/-0.263	0.266/-0.182	0.390/-0.232			0.591/-0.267		
				powder diffraction data (298 K)				
a, Å	12.17799(19)	14.3780(4)	19.8646(8)	10.1462(5)	3.64304(8)	20.2359(10)	9.8770(3)	18.91(4)
b, Å	3.73926(7)	9.4023(3)	3.74868(11)	13.2552(8)	9.2819(2)	5.8288(2)	12.4749(3)	7.769(11)
c, Å	11.56377(19)	8.7612(4)	8.7084(4)	9.6767(5)	9.3249(3)	12.4410(4)	5.64751(19)	5.032(6)
β, °				118.9905(15)	100.5105(16)	98.065(3)	96.102(3)	
V, Å^3	526.576(15)	1184.40(7)	648.48(4)	1138.35(10)	310.027(14)	1452.91(10)	691.91(3)	739(2)
d_{calc}, g·cm^{-3}	1.616	1.605	1.650	1.682	1.704	1.720	1.805	1.825

[a] Ref.[14]

[14] A. A. Voronin, I. V. Fedyanin, A. M. Churakov, A. N. Pivkina, N. V. Muravyev, Y. A. Strelenko, M. S. Klenov, D. B. Lempert and V. A. Tartakovsky, 4*H*-[1,2,3]Triazolo[4,5-*c*][1,2,5]oxadiazole 5-oxide and Its Salts: Promising Multipurpose Energetic Materials, *ACS Appl. Energ. Mat.*, 2020, **3**(9), 9401–9407. https://doi.org/10.1021/acsaem.0c01769

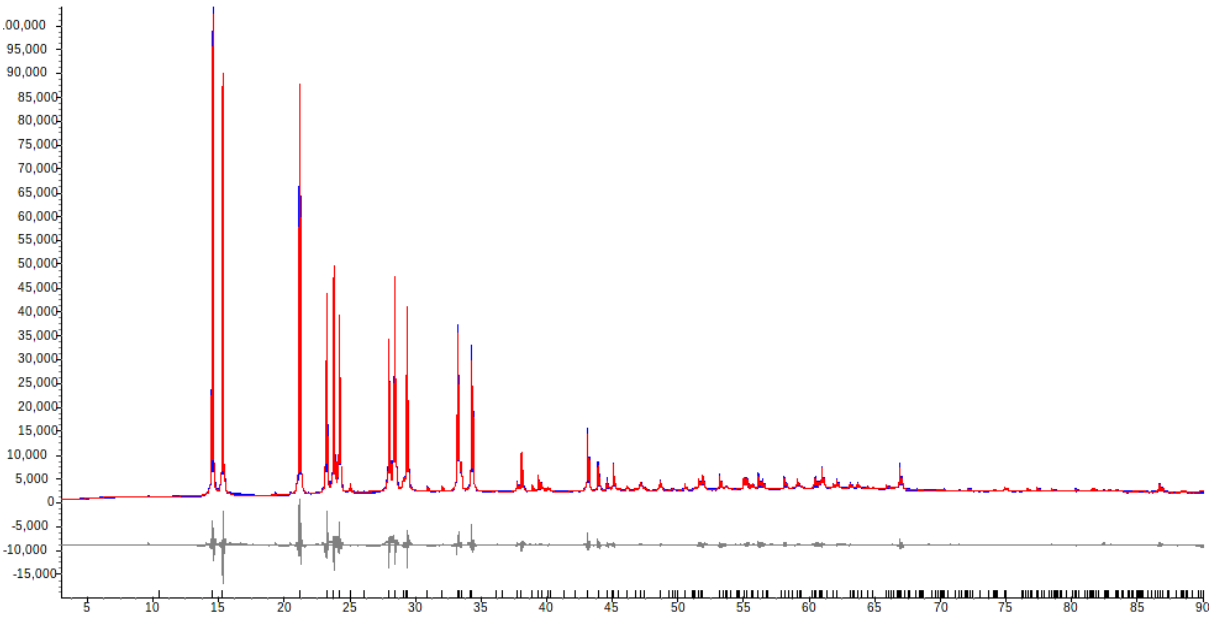

Fig. SIF1. Observed (blue line) and calculated (red line, Pawley fit, Rwp=0.0635) powder diffraction patterns for the salt **2a**.

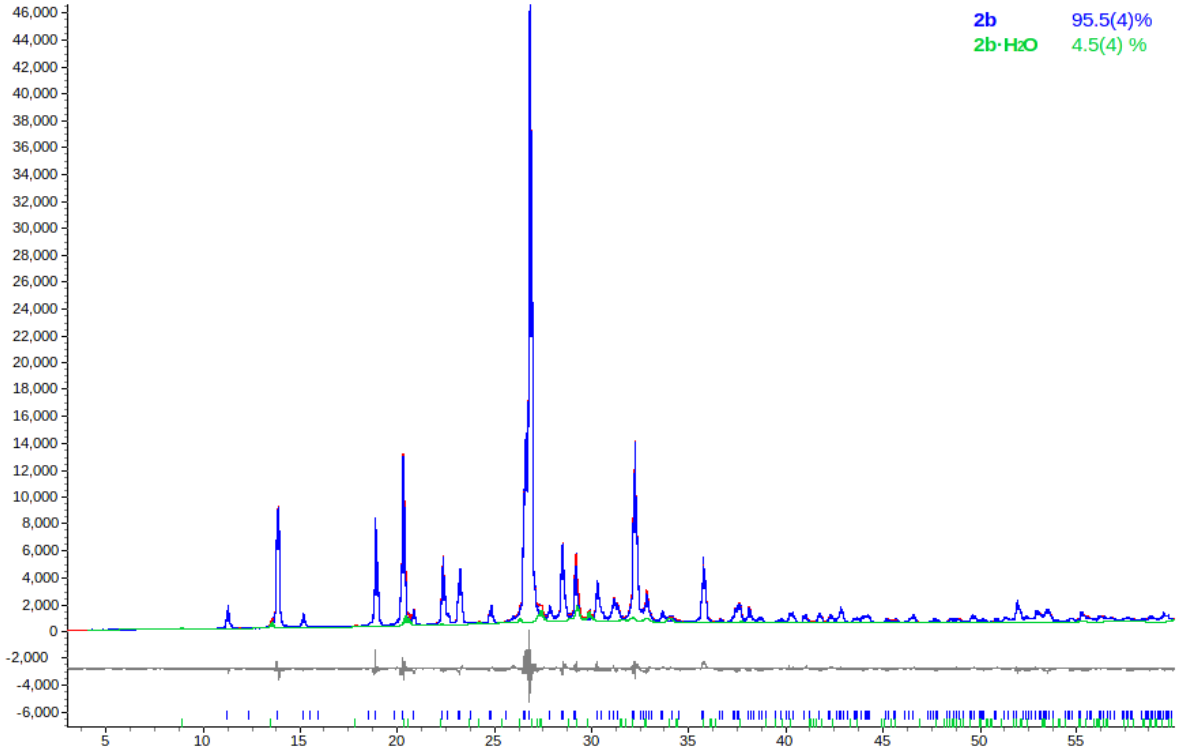

Fig. SIF2. Powder diffraction pattern for the salt **2b** (blue line) and the admixture of the salt **2b·H2O** (green line). Red line is the calculated pattern (constrained Rietveld fit, Rwp=0.0622, Rbragg= 0.018 for 2b). The phase ratio (96:4) was calculated from the corresponding areas of the curves.

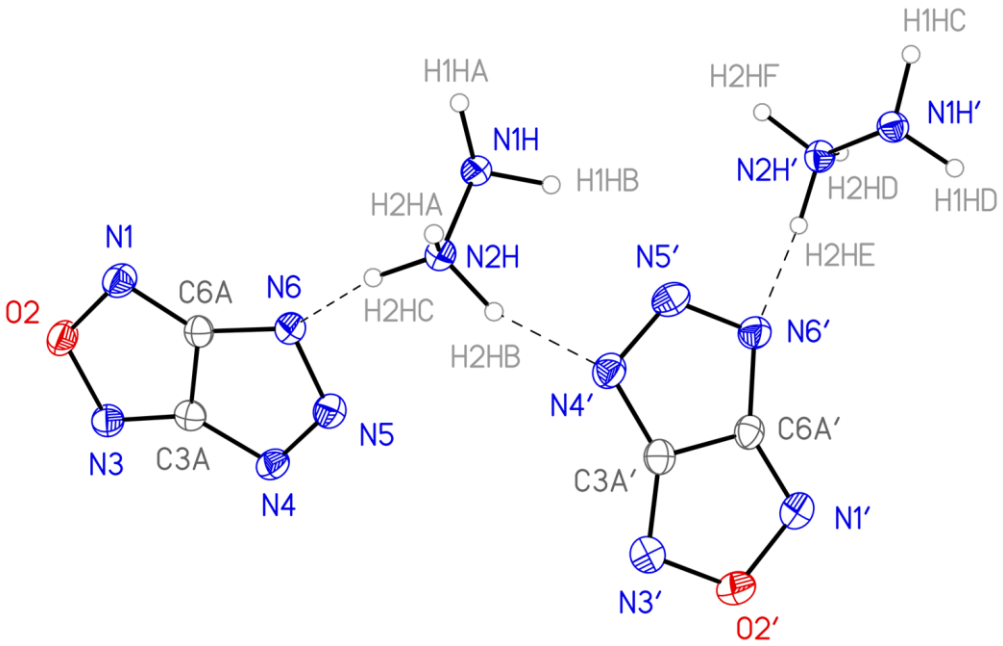

Fig. SIF3. General view of the components (two sets of crystallographically independent anions and cations) of the salt **2b** in the crystal. Anisotropic displacement parameters for non-H atoms are drawn at the 50% probability level.

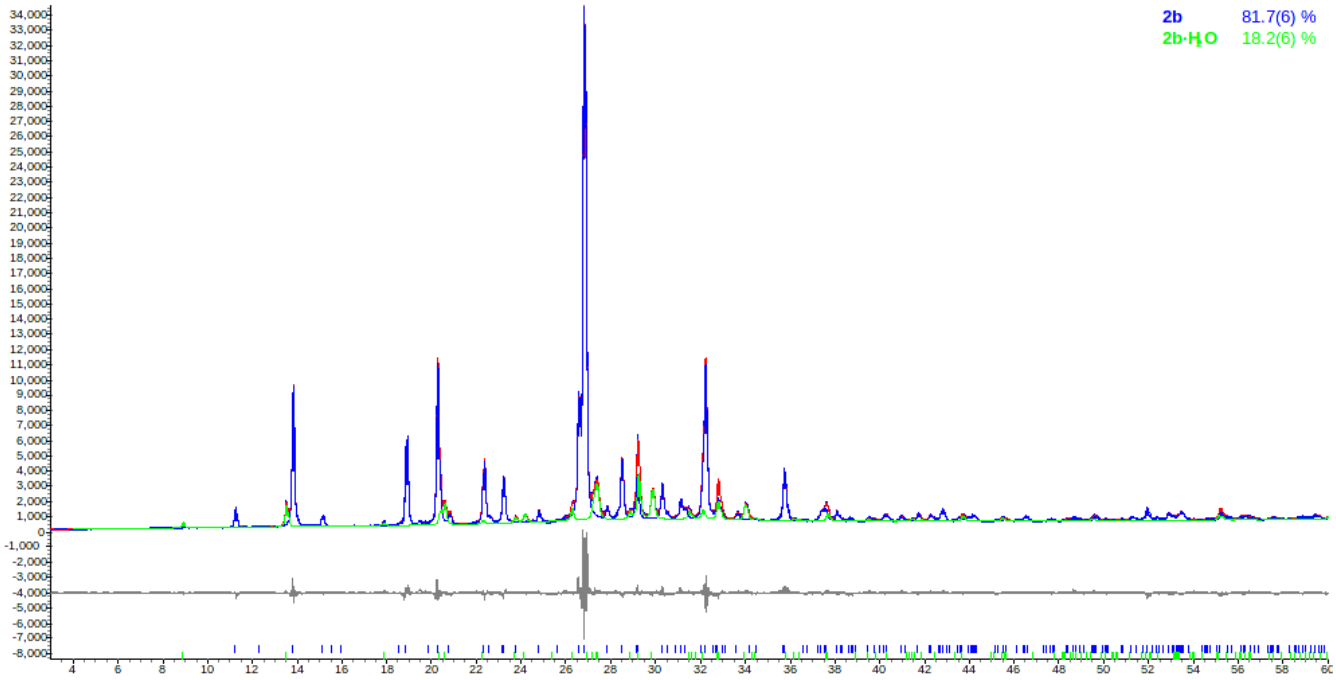

Fig. SIF4. Powder diffraction pattern of an arbitrary sample of the salt **2b** (blue line) and the admixture of the salt **2b·H₂O** (green line). Red line is the calculated pattern (constrained Rietveld fit, R_{wp}=0.064, R_{bragg}= 0.026 and 0.027 for **2b** and **2b·H₂O**). The phase ratio (81:19) was calculated from the corresponding areas of the curves.

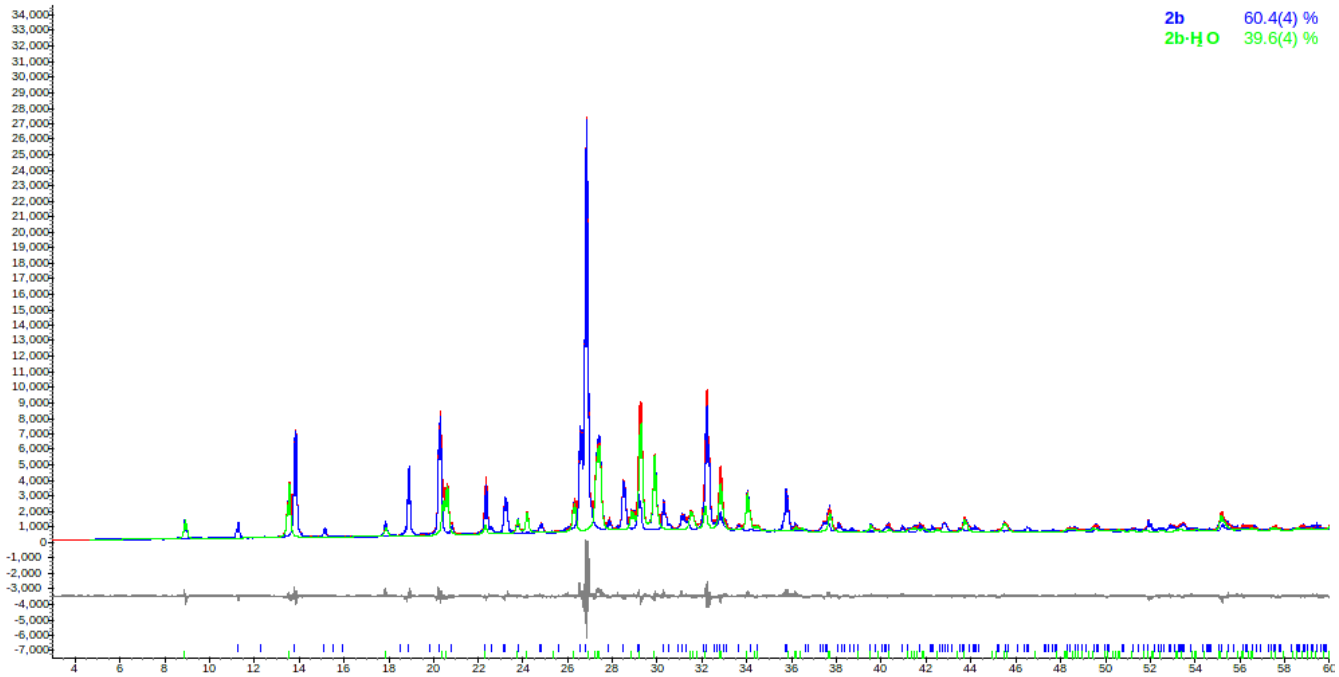

Fig. SIF5. Powder diffraction pattern of the same sample as in **Fig. SIF3,** but after 20 hours. The phase ratio (61:39) was calculated from the corresponding areas of the curves.

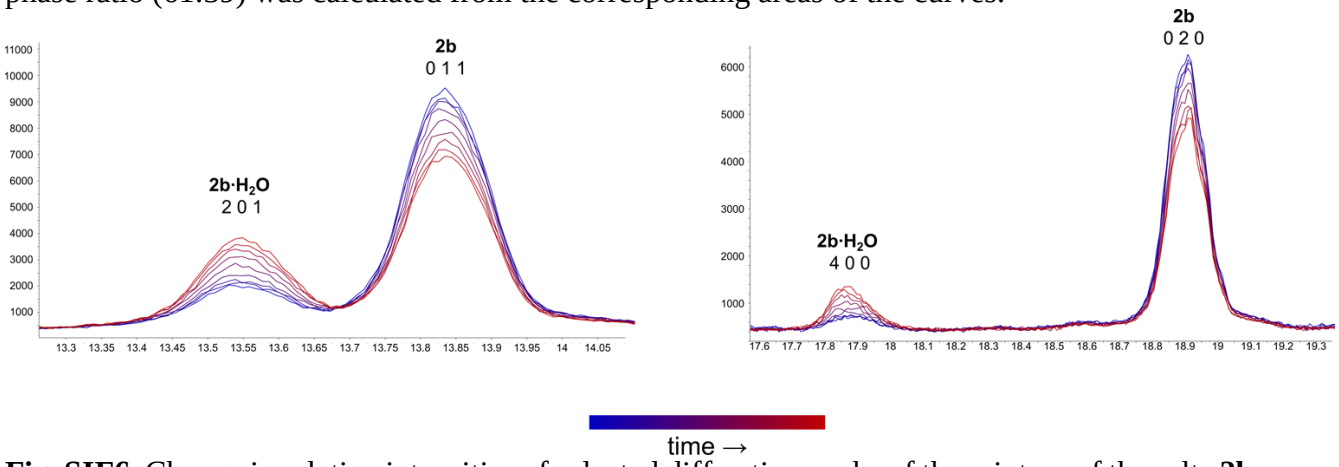

Fig. SIF6. Change in relative intensities of selected diffraction peaks of the mixture of the salts **2b** and its hydrate form **2b·H₂O**, for the sample depicted in **Figs. SIF2 and SIF3.** Each of the nine curves curve represents a single run that took approximately 2.5 hours at ambient conditions. The weight of the sample, which was deposited on a silicon sample holder of ⌀ = 20mm, was ca. 30 mg.

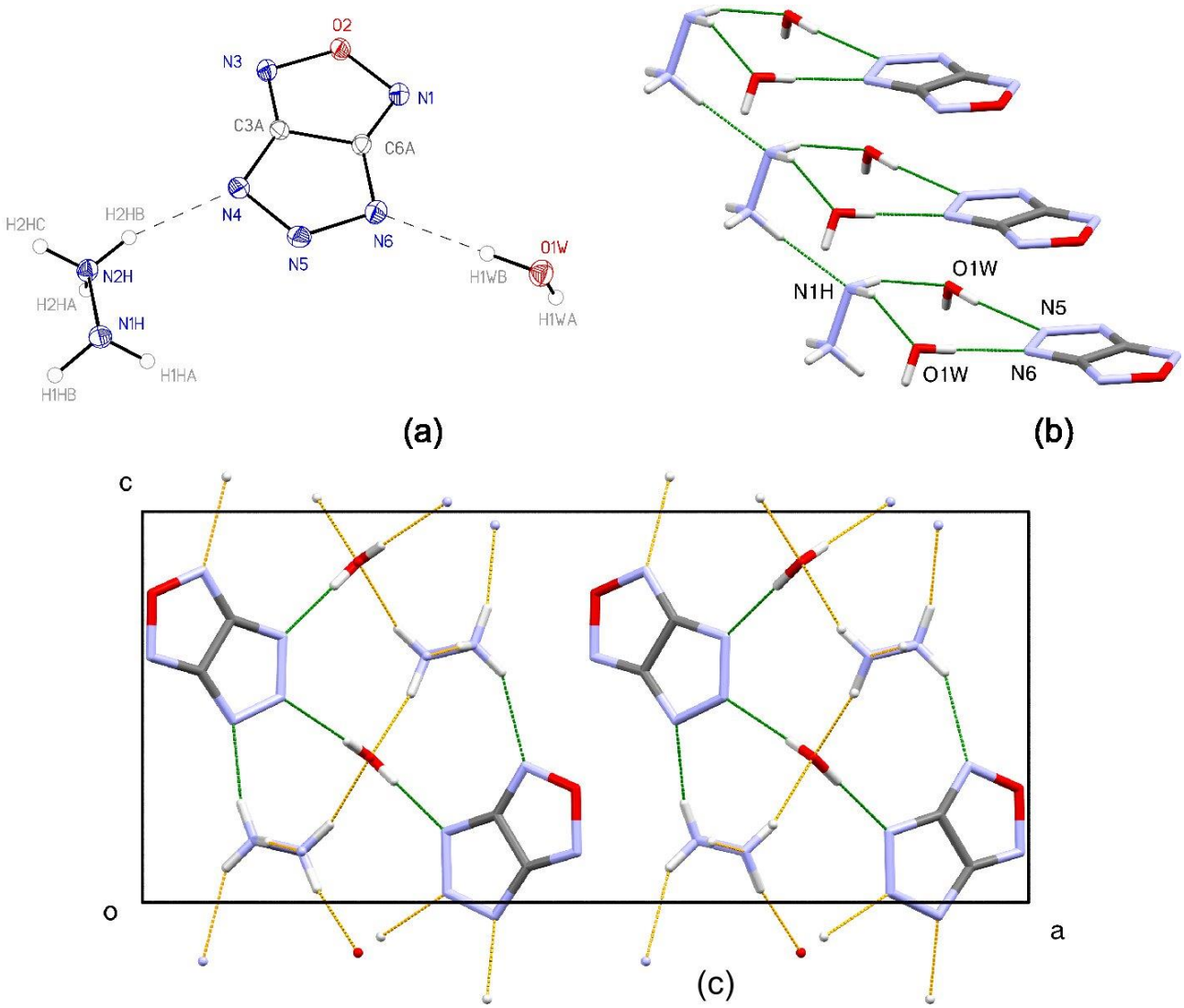

Fig. SIF7. (a) General view of the components of **2b·H₂O** in the crystal. Anisotropic displacement parameters for non-H atoms are drawn at the 50% probability level. (b) Fragment of the crystal packing of **2b·H₂O** demonstrating the formation of cationic chains and H-bonds with water molecules. (c) Fragment of the crystal packing of **2b·H₂O**, view along the crystallographic *b* axis.

The mono-hydrate **2b·H₂O** (sp. gr. $Pca2_1$) crystallizes with one crystallographically independent moiety of each type (Z'=1). Interestingly, the supramolecular synthon, the cationic H-bonded chains, also present in this structure, and the cations having staggered conformation are related by translation along *b* direction (N···N 2.935 Å, N-H···N 176°). The water molecule provides two additional donor and two acceptor sites available for H-bonding, and acts as an acceptor by bonding with both H atoms of non-protonated part of the cation (N···O 2.970(3) and 2.977(3) Å, N-H···O 160 and 151°). The H atoms of water molecules and -NH_3 fragment form H-bonds with all available N atoms of both heterocyclic rings. The anion···anion interactions include

π-stacking in infinite ladder-like stacks, and O···N contacts between nearly parallel molecules rotated relative to each other by 110° similar to those in **2a**. (Fig. SIF7 in ESI). In contrast to pure **2b**, all H-bonds in the hydrate are weak (the strongest is O-H···N bond with 2.842(3) Å.

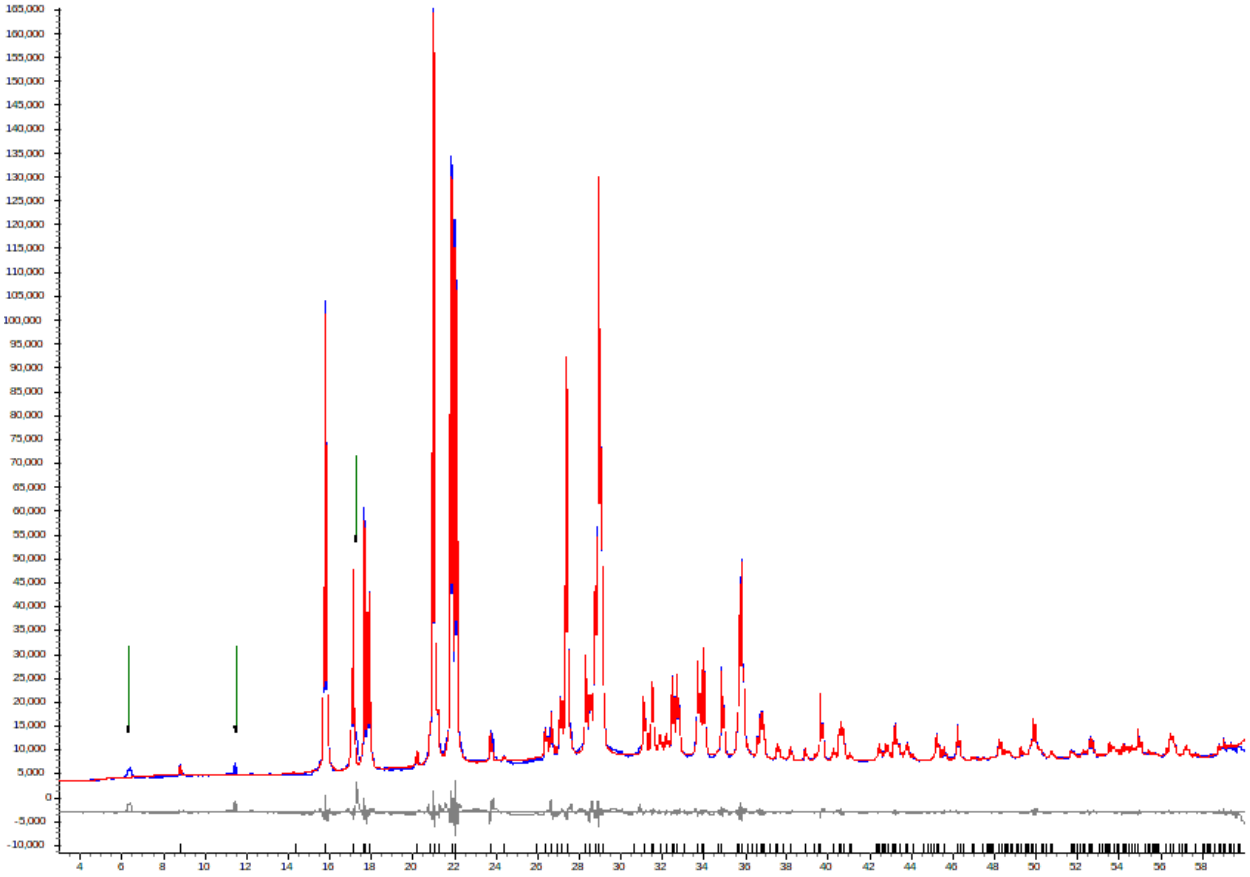

Fig. SIF8. Observed (blue line) and calculated (red line, Pawley fit, Rwp=0.0651) powder diffraction patterns for the salt **6b-I.** The most intense peaks, marked by green arrows, belong to an unidentified admixture phase, the amount of which, estimated from the peak area, does not exceed 1.5%.

Details of crystal structure solution of the polymorph 6b-II.

While the bulk sample of **6b** was almost phase pure, containing less than 0.5% of the unidentified admixture, the PXRD analysis of the sample obtained by recrystallization from acetonitrile showed that the prevailing phase is different from the one discussed above (**6b-I**), while the latter is still present in the sample as a minor phase. Indexing of the peaks corresponding to the major phase (**6b-II**) showed that its density is considerably higher than that of **6b-I**. Considering the multinuclear NMR, elemental analysis data and the thermal behavior of the sample discussed below, we assume that **6b-II** is indeed a second polymorphic form of salt **6b**. In

fact, we were able to obtain a crystal structure solution from the PXRD data of the mixed-phase sample, which partially confirms its structure. The difference in density between two forms may look suspicious, nevertheless it occurs for polymorphic forms of energetic compounds (CL-20 is a known example).

The peaks of the diffraction pattern of the bulk sample **6b** (obtained by recrystallization from acetonitrile) that did not fit the polymorphic form **6b-I** were indexed using the SVD (singular value decomposition) indexing algorithm[15] as implemented in the Bruker TOPAS 5.0 software[16]. The space group was determined by analysis of systematic absences. Then, the part of the diffraction curve belonging to the hypothetical structure **6b-II**, calculated by Pawley fit, was saved and used for the structure solution in direct space by the parallel tempering approach implemented in the FOX package[17]. The solution was easily found, and the resulting coordinates were used for the constrained Rietveld fit below (Fig. SIF10).

We understand that the solution may be incorrect due to the relatively poor quality of the diffraction data and the high relative amount of the phase **6b-I** in the sample (estimated at 15-20% by areas under the curves). The restrained Rietveld refinement cannot be performed for the same reasons. Unfortunately, the pure sample of **6b-II** cannot be obtained by heating to the phase transition temperature, as this temperature is too close to the decomposition equilibrium and the transitions are either not complete or the sample starts to degrade. Nevertheless, we provide figures of crystal packing of the hypothetical structure obtained as FOX solution below (Fig. SIF11), since its crystal packing is logical and in something similar to **6b-I**.

[15] A. A. Coelho, Indexing of powder diffraction patterns by iterative use of singular value decomposition, *J. Appl. Crystallogr.*, 2003, **36**, 86–95. https://doi.org/10.1107/S0021889802019878

[16] A. A. Coelho, TOPAS and TOPAS-Academic: an optimization program integrating computer algebra and crystallographic objects written in C++, *J. Appl. Crystallogr.*, 2018, **51**, 210–218. https://doi.org/10.1107/S1600576718000183

[17] V. Favre-Nicolin and R. Černý, FOX, `free objects for crystallography': a modular approach to ab initio structure determination from powder diffraction, *J. Appl. Crystallogr.*, 2002, **35**, 734–743. https://doi.org/10.1107/S0021889802015236

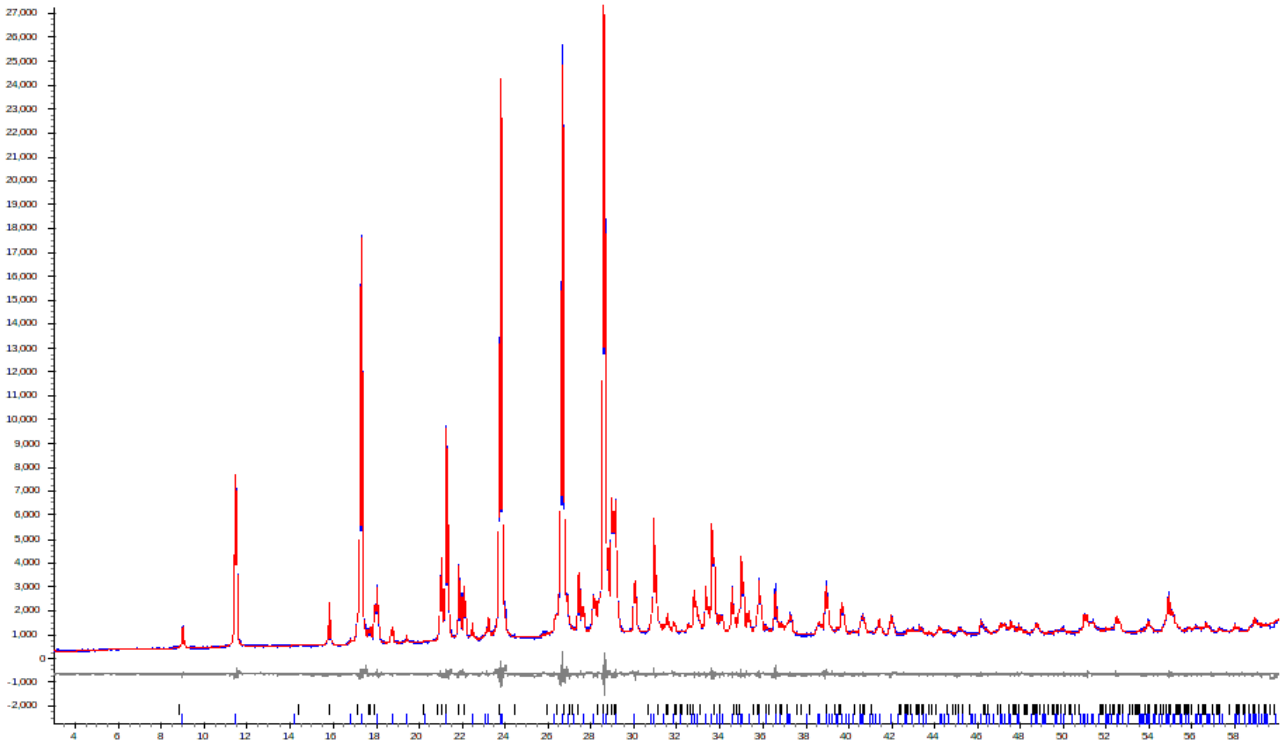

Fig. SIF9. Observed (blue line) and calculated (red line, Pawley fit, Rwp=0.0321) powder diffraction patterns for the mixture of polymorphic salts **6b-I** and **6b-II**.

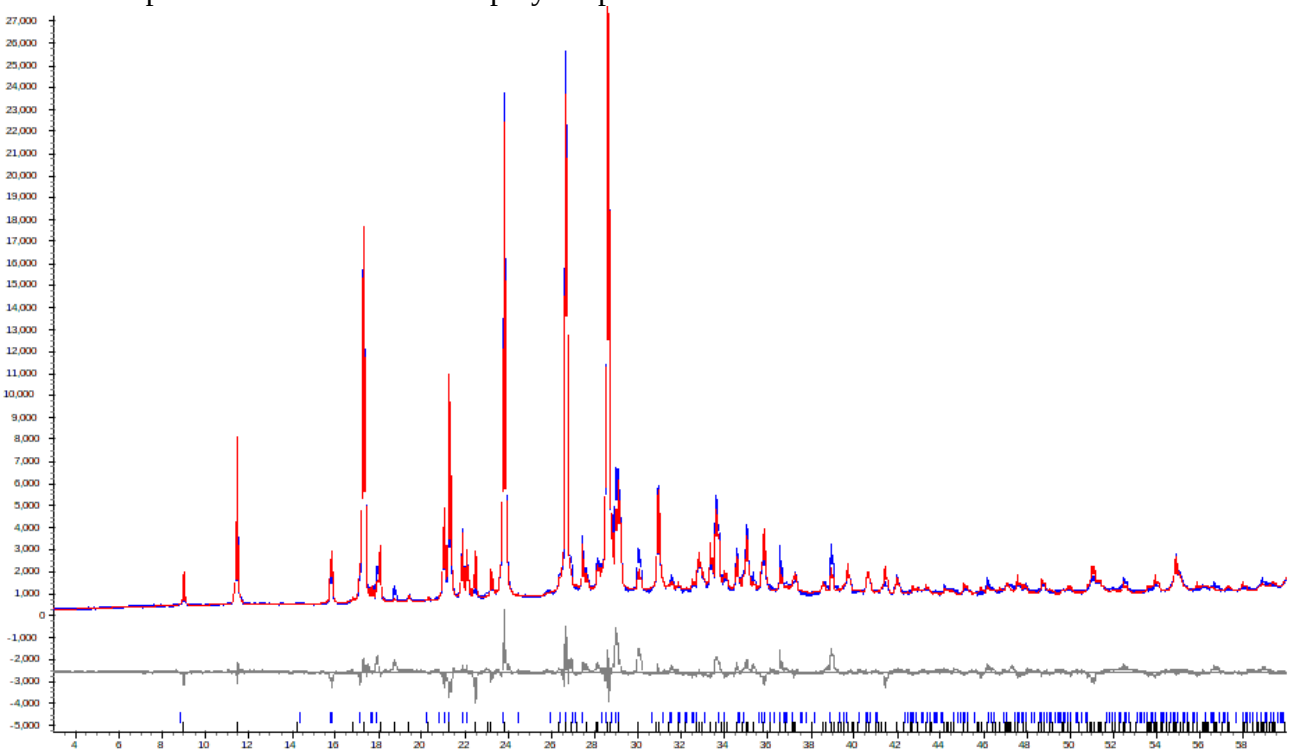

Fig. SIF10. Observed (blue line) and calculated powder diffraction patterns for the mixture of polymorphs **6b-I** and **6b-II** (the same experimental pattern as in Fig. SIF9). The curve is calculated using the constrained Rietveld refinement, with fixed fractional atomic coordinates of **6b-I** taken from the single-crystal refinement, and those of **6b-II** from the FOX solution.

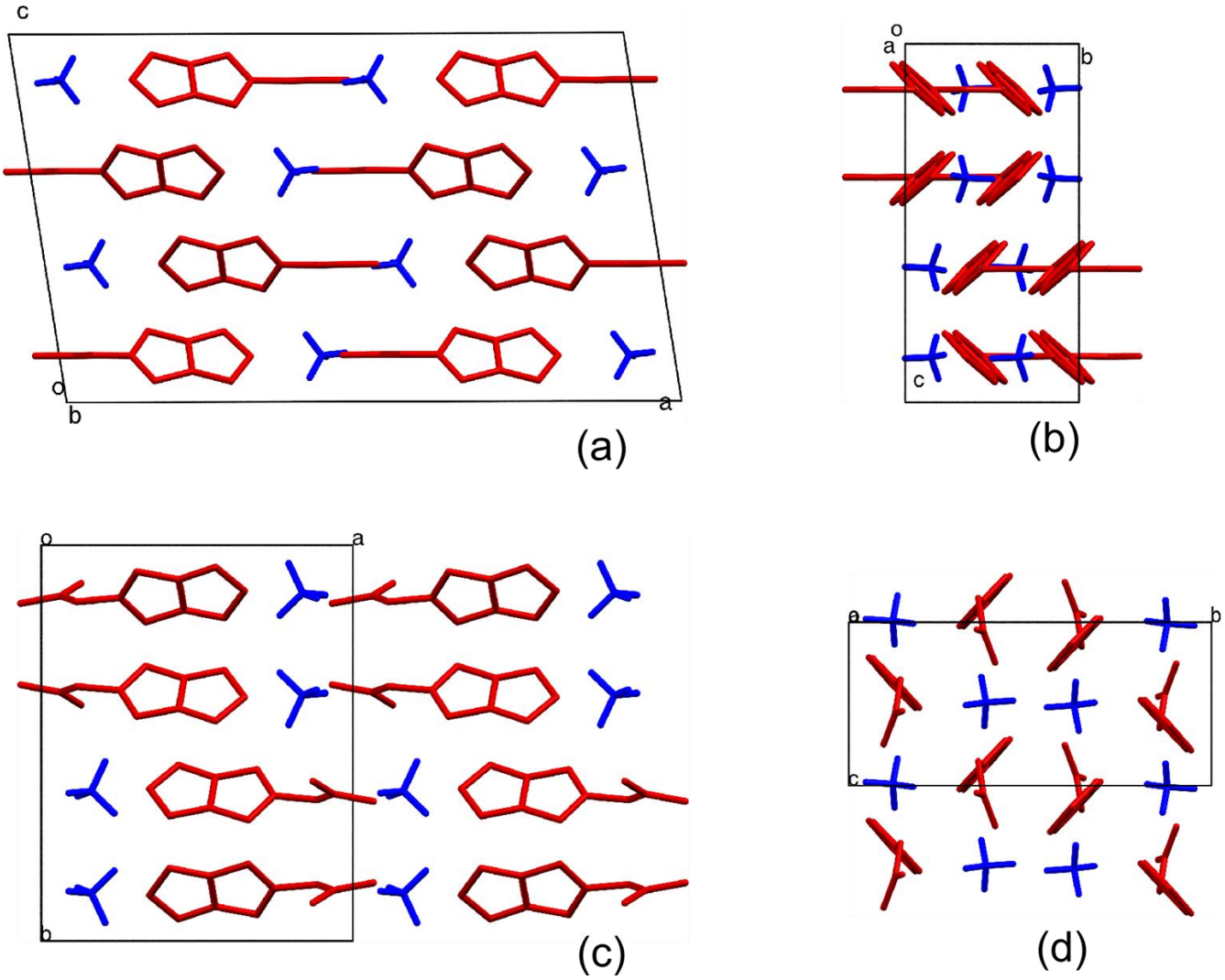

Fig. SIF11. Comparison of crystal packing of polymorphic salts **6b-I** (top, single-crystal experiment) and **6b-II** (bottom, FOX solution). Close distance between the ammonium cations is the visualization artifact, the real N···N distance exceeds 4 Å.

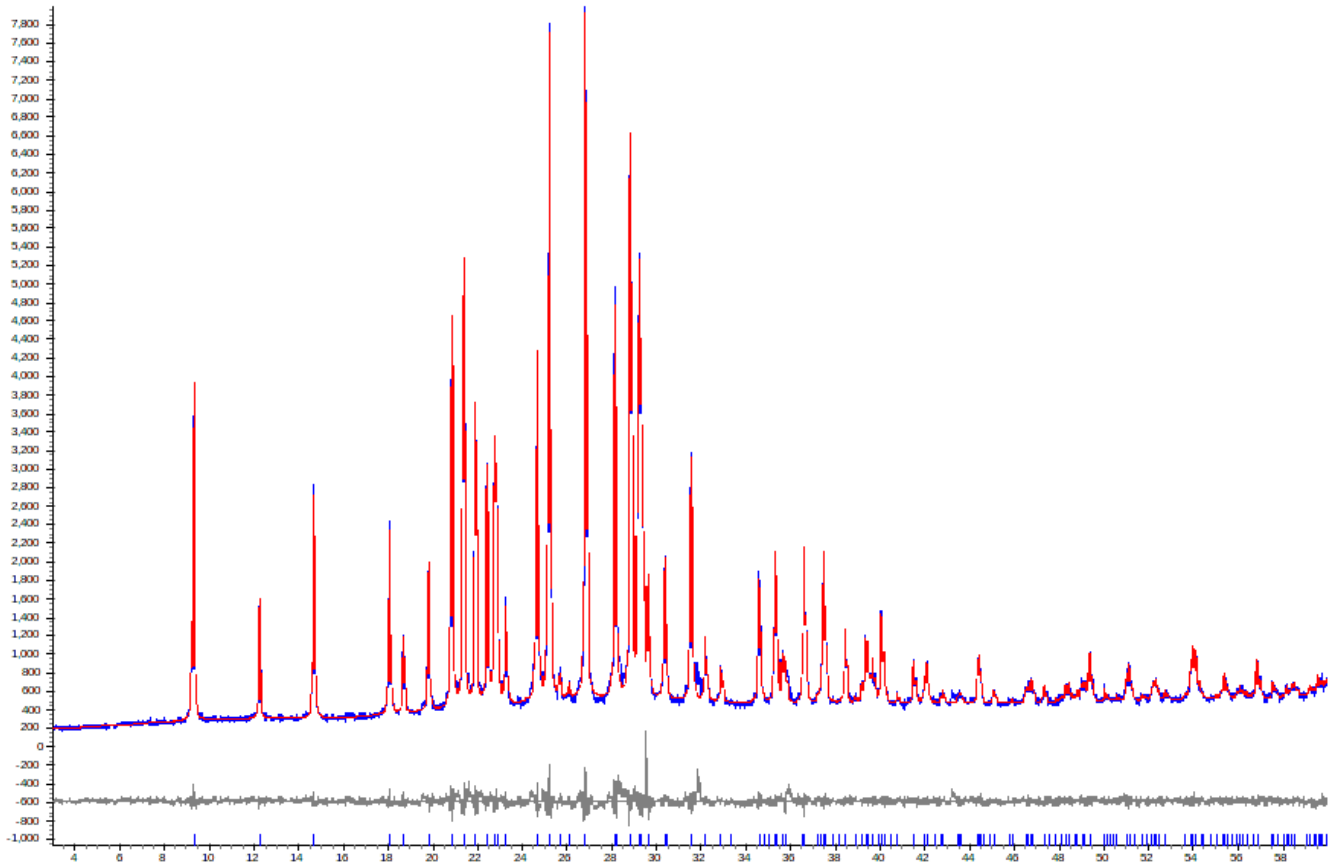

Fig. SIF12. Observed (blue line) and calculated (red line, Pawley fit, Rwp=0.0618) powder diffraction patterns for the salt **6d**.

Table SIF2. Bond lengths (Å) in the anions of all salts discussed in the paper. Capital letters in row headings correspond to crystallographically independent anions. Data for **2b** have not been included because bond lengths were constrained in this structure.

	2b-A	**2b-B**	**2b·H_2O**	**3b-A**	**3b-B**	**3b-C**	**3b-D**	**3c**	**6b-I**
N1-O2	1.409(4)	1.405(4)	1.402(2)	1.415(3)	1.416(4)	1.416(3)	1.411(3)	1.419(2)	1.4075(9)
O2-N3	1.406(4)	1.411(5)	1.408(2)	1.423(3)	1.415(4)	1.422(3)	1.417(3)	1.414(2)	1.3968(9)
N1-C6A	1.307(5)	1.305(5)	1.307(3)	1.297(4)	1.310(3)	1.301(4)	1.311(4)	1.306(3)	1.3152(10)
N3-C3A	1.315(5)	1.316(5)	1.316(3)	1.313(4)	1.304(4)	1.305(4)	1.312(4)	1.306(3)	1.3137(11)
C3A-N4	1.371(4)	1.360(5)	1.360(3)	1.356(4)	1.376(4)	1.359(4)	1.369(4)	1.364(3)	1.3617(10)
N6-C6A	1.362(5)	1.366(5)	1.368(3)	1.368(4)	1.369(4)	1.360(4)	1.367(4)	1.366(3)	1.3630(10)
N4-N5	1.335(4)	1.342(4)	1.343(3)	1.363(3)	1.359(3)	1.366(3)	1.350(3)	1.357(2)	1.3381(9)
N5-N6	1.348(4)	1.340(5)	1.343(2)	1.355(3)	1.347(3)	1.359(3)	1.340(3)	1.364(2)	1.3357(9)
C3A-C6A	1.404(5)	1.402(5)	1.408(3)	1.426(3)	1.418(4)	1.420(4)	1.409(4)	1.418(3)	1.4110(11)
N5-O/N				1.250(3)	1.270(3)	1.238(3)	1.274(3)	1.252(2)	1.3766(9)

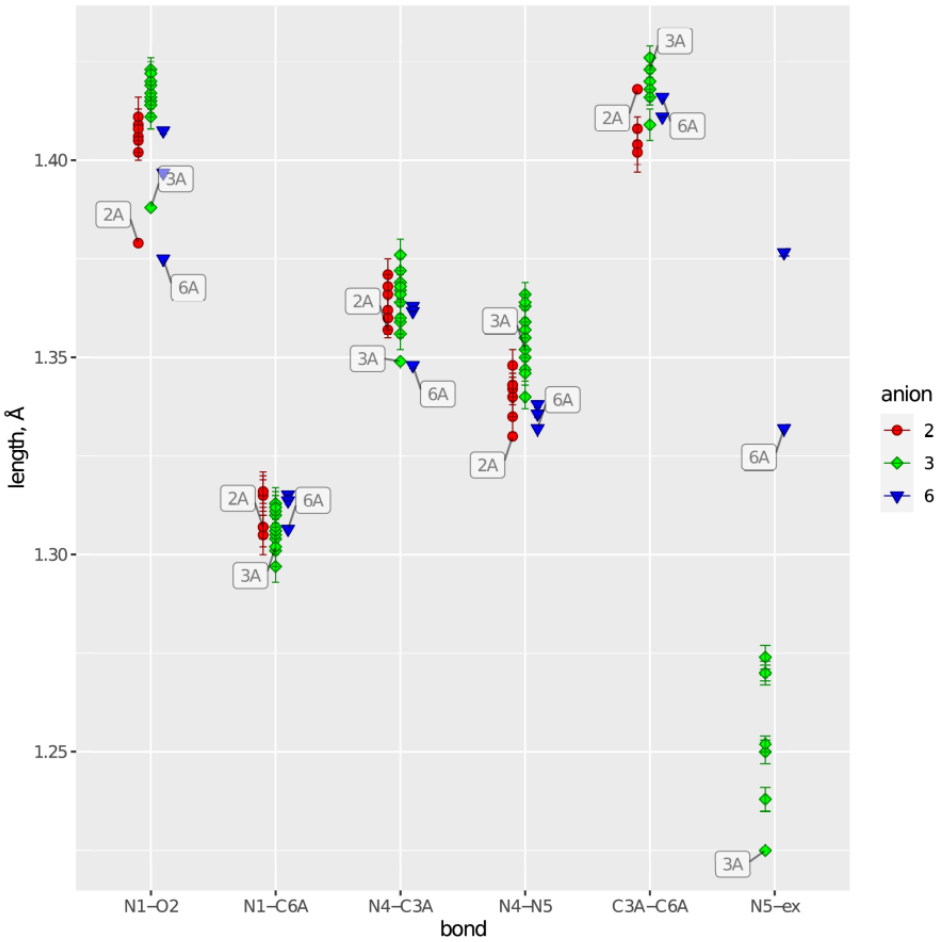

Fig. SIF13. Graphical representation of the experimental bond lengths in anions **2**, **3**, and **6**, and the bond lengths calculated for isolated anions by the PBE0-def2/TZVPP method. The bond lengths are grouped under the assumption of C_{2v} symmetry of the heterocyclic moiety. The DFT-calculated values 2A, 3A and 6A are highlighted.

Combustion calorimetry

The measurements were performed on a precision automatic combustion calorimeter with an isothermal shell designed by the Laboratory of Thermodynamics of High-Energy Systems of the Federal Research Center of Chemical Physics named after N. N. Semenov of the Russian Academy of Sciences for the combustion of energetic compounds.[18]

Basic design features of the calorimeter used in this study: 1) small heat equivalent (~500 cal·degree^{-1}) with a large volume of bomb (200 cm^3); 2) simple installation bomb calorimeter – just remove the cap shell and the calorimetric vessel, drop the bomb and close the cover; 3) continuously thermostatic shell; 4) permanently fixed to the sheath liquid hermetic calorimeter vessel is in the form of a glass with double walls (calorimeter constant volume of fluid that delivers constant heat equivalent); 5) low measurement error. The calorimeter allows one to measure the thermal effect of the combustion reaction of substances with an extended uncertainty of 0.01–0.02%. Calibration of the calorimeter was carried out with the reference benzoic acid of the K-1 brand produced by the D. I. Mendeleev Institute of Metrology. The combustion energy of benzoic acid under standard conditions was 6322.6 ± 1.2 cal·g^{-1}. The absence of a systematic error in calorimetric measurements was controlled by burning secondary reference substances-succinic and hippuric acids, whose combustion energies on this calorimeter were 3020.3 ± 0.6 cal·g^{-1} (0.02%) and 5631.4 ± 3.4 cal·g^{-1} (0.06%), respectively. Samples of the studied compounds **2a,b, 3b,c** and **6b,d** were burned in a platinum crucible. Pressed tablets of substances were weighed on Bunge microanalytic scales with an error of 2·10^{-6} g. The suspended sample of the substance was placed in a calorimetric bomb and filled with oxygen. The initial oxygen pressure during the combustion of all substances is about 30 atm (3 MPa). Before the experiment, 1 mL of distilled water was injected into the bomb to create a saturated vapor pressure and dissolve the nitrogen oxides formed during the combustion process.

The samples were ignited with a cotton thread, which in turn was ignited by incandescent platinum wire (diameter 0.3 mm) with a dosed pulse of current supplied from a special device. The combustion energy of cotton yarn was measured in a series of seven experiments and amounted to 3968.9 ± 1.6 cal·g^{-1}. When determining the combustion energy, corrections for the thermal effects of nitric acid formation, heat exchange of a calorimetric vessel with an isothermal shell, and the

[18] Ya. O. Inozemtsev, A. B. Vorob'ev, A. V. Inozemtsev and Yu. N. Matyushin, A method for estimating thermochemical properties of salt compounds, *Combustion and Explosion*, 2014, **7**, 260–270.

combustion energy of the auxiliary substance and cotton thread were taken into account. A detailed procedure for preparing samples and conducting an incineration experiment was described earlier.[19]

The combustion energies ($-\Delta U'_B$, cal·g^{-1}) under calorimetric bomb conditions for the studied salts **2a,b, 3b,c** and **6b,d** are summarized in Table SIF3.

Table SIF3. Calorimetric determination of the combustion energies of compounds 2a,b, 3b,c and 6b,d.

N[a]	m[b] g	□T[c] °C	Q[d] cal	q_a[e] cal	q_i[f] cal	q_N[g] cal	q_{cot}[h] cal	$-U'_B$[i] cal·g^{-1}
Compound **2a NH_4TF**								
1	0.060704	2.02722	1089.91	877.56	7.26	1.73	9.10	3200.2
2	0.065313	2.06303	1109.17	882.11	7.28	1.88	8.76	3202.1
3	0.063847	2.06006	1107.57	885.32	7.24	1.82	8.98	3198.4
4	0.067021	2.04624	1100.14	867.52	7.30	1.91	8.69	3203.8
5	0.069516	2.10609	1132.32	891.51	7.21	1.98	9.21	3199.4
								$-\Delta U'_B$ = 3200.8 ± 2.2 cal·g^{-1}
Compound **2b N_2H_5TF**								
1	0.064126	2.16540	1164.44	956.73	7.23	2.18	9.14	3307.1
2	0.060904	2.15539	1159.06	884.94	7.28	2.08	8.92	3311.6
3	0.061472	2.02779	1090.22	868.39	7.24	2.09	9.06	3309.5
4	0.062163	2.00086	1075.74	852.17	7.30	2.11	8.76	3304.2
5	0.063871	2.07392	1115.02	885.32	7.28	2.17	9.12	3305.6
								$-\Delta U'_B$ = 3307.6 ± 2.0 cal·g^{-1}
Compound **3b NH_4TFO**								
1	0.095621	2.10345	1131.13	850.48	7.23	2.48	9.01	2739.2
2	0.098772	2.26869	1219.99	931.43	7.32	2.57	8.43	2736.0
3	0.101893	2.13897	1150.23	852.15	7.25	2.65	8.81	2741.8
4	0.052044	1.89220	1017.53	857.12	7.24	1.35	9.32	2738.1
5	0.050816	2.02665	1089.84	932.86	7.21	1.30	9.18	2740.9
								$-\Delta U'_B$ = 2739.2 ± 2.6 cal·g^{-1}
Compound **3c N_2H_5TFO**								
1	0.064127	2.16540	1164.44	956.73	7.23	2.28	9.14	2948.2
2	0.062074	2.15539	1159.06	957.93	7.32	2.21	8.52	2949.4
3	0.069778	2.16426	1163.83	938.99	7.26	2.48	9.18	2951.1
4	0.070437	2.17339	1168.74	942.06	7.28	2.50	9.23	2948.3
5	0.070022	2.16638	1164.97	939.21	7.24	2.48	9.42	2950.8
								$-\Delta U'_B$ = 2949.6 ± 1.6 cal·g^{-1}
Compound **6b NH_4TFNA**								
1	0.079054	2.23194	1199.98	994.60	7.32	2.21	7.72	2379.8
2	0.060740	2.29055	1231.56	1069.73	7.22	1.74	8.36	2379.2
3	0.061517	2.18896	1176.87	1013.13	7.27	1.76	8.47	2377.3
4	0.064051	2.20592	1185.99	1016.11	7.23	1.79	8.65	2376.4
5	0.062972	1.95898	1053.23	885.58	7.30	1.78	8.41	2384.6
								$-\Delta U'_B$ = 2379.5 ± 3.7 cal·g^{-1}

[a] Ordinal number of the experiment. [b] Weight of the sample of compound in vacuum. [c] Corrected temperature rise in the calorimeter. [d] Heat measured in the experiment. [e] Heat of combustion of the auxiliary substance (benzoic acid). [f] Ignition energy. [g] Correction for the formation of nitric acid. [h] Heat of combustion of the cotton thread. [i] Combustion energy of a compound in the bomb.

[19] T. S. Kon'kova, Yu. N. Matyushin, E. A. Miroshnichenko and A. B. Vorob'ev, Thermochemical properties of dinitramidic acid salts, *Russ. Chem. Bull.*, 2009, **58**(10), 2020–2027. https://doi.org/10.1007/s11172-009-0276-z

The standard enthalpy of combustion and formation of salts 2a,b, 3b,c and 6b

The reactions of combustion of compounds **2a,b**, **3b,c** and **6b** are:

2a: $C_2H_4N_6O_{(cr)} + 2.5O_{2(g)} = 2CO_{2(g)} + 2H_2O_{(l)} + 3N_{2(g)}$

2b: $C_2H_5N_7O_{(cr)} + 2.75O_{2(g)} = 2CO_{2(g)} + 2.5H_2O_{(l)} + 3.5N_{2(g)}$

3b: $C_2H_4N_6O_{2(cr)} + 2O_{2(g)} = 2CO_{2(g)} + 2H_2O_{(l)} + 3N_{2(g)}$

3c:$2C_2H_5N_7O_{2(cr)} + 2.25O_{2(g)} = 2CO_{2(g)} + 2.5H_2O_{(l)} + 3.5N_{2(g)}$

6b:$C_2H_4N_8O_{3(cr)} + 1.5O_{2(g)} = 2CO_{2(g)} + 2H_2O_{(l)} + 4N_{2(g)}$

cr, g, and l correspond to the crystalline, gaseous, and liquid states, respectively.

The standard enthalpies of formation (SEOF) of compounds **2a,b**, **3b,c** and **6b** were calculated based on the standard enthalpies of combustion using equations:

2a: $\Delta H°_f[C_2H_4N_6O]_{(cr)} = 2\Delta H°_f[CO_2]_{(g)} + 2\Delta H°_f[H_2O]_{(l)} - \Delta H°_c$

2b: $\Delta H°_f[C_2H_5N_7O]_{(cr)} = 2\Delta H°_f[CO_2]_{(g)} + 2.5\Delta H°_f[H_2O]_{(l)} - \Delta H°_c$

3b: $\Delta H°_f[C_2H_4N_6O_2]_{(cr)} = 2\Delta H°_f[CO_2]_{(g)} + 2\Delta H°_f[H_2O]_{(l)} - \Delta H°_c$

3c: $\Delta H°_f[C_2H_5N_7O_2]_{(cr)} = 2\Delta H°_f[CO_2]_{(g)} + 2.5\Delta H°_f[H_2O]_{(l)} - \Delta H°_c$

6b: $\Delta H°_f[C_2H_4N_8O_3]_{(cr)} = 2\Delta H°_f[CO_2]_{(g)} + 2\Delta H°_f[H_2O]_{(l)} - \Delta H°_c$

$\Delta H°_c$ – the standard enthalpy of combustion of the corresponding compound, kcal·mol^{-1}, $\Delta H°_f$ – the standard enthalpy of its formation, kcal·mol^{-1}.

Reference values of the SEOF of combustion products are taken from the CODATA Key Values for Thermodynamics table[20] and are equal to:

$\Delta H°_f[CO_2]_{(g)} = -94.051 \pm 0.031$ kcal·mol^{-1}

$\Delta H°_f[H_2O]_{(l)} = -68.315 \pm 0.009$ kcal·mol^{-1}.

Table SIF4. Standard thermochemical characteristics for compounds 2a,b, 3b,c and 6b,d.

Salt	$-\Delta U_B$ [a] cal·g^{-1}	$-\Delta H°_c$ [b] kcal·mol^{-1}	$\Delta H°_f$ [c] kcal·mol^{-1}	$\Delta H°_f$ [c] kcal·kg^{-1}
2a	3200.8 ± 2.2	–407.8 ± 0.3	**83.1 ± 0.3**	**649.2 ± 2.3**
2b	3307.6 ± 2.0	–470.9 ± 0.3	**112.0 ± 0.3**	**783.2 ± 2.3**
3b	2739.2 ± 2.6	–403.3 ± 0.4	**78.6 ± 0.4**	**530.8 ± 2.7**
3c	2949.6 ± 1.6	–466.7 ± 0.3	**107.8 ± 0.3**	**677.8 ± 1.9**
6b	2379.5 ± 3.7	–444.3 ± 0.7	**119.6 ± 0.7**	**635.8 ± 3.7**
6d	—	—	**146.8**[d]	**731.3**[d]

[a] Energy of combustion. [b] Standard enthalpy of combustion. [c] Standard enthalpy of formation. [d] Calculated values (details see below)

[20] J. D. Cox, D. D. Wagman, V. A. Medvedev Eds., *CODATA key values for thermodynamics. Final Report of the CODATA Task Group on Key Values for Thermodynamics*, New York, Washington, Philadelphia, London, 1989.

Theoretical study. Estimation of the enthalpy of formation of hydrazinium salt 6d

All calculations were performed using the Gaussian 09[21] (Revision D.01) and Molpro 2010[22] programs package. Geometry optimization and vibrational frequency calculation of all species were carried out at the MP2/6-31G(d,p) level. The optimized geometries were used as inputs for further Gaussian-4 (G4)[23] and W1-F12[24] levels of theory applied to the atomization energy approach[25]. The calculation *via* the atomization reaction involves the use of experimental enthalpies of formation of gaseous atoms at T = 0 K and thermal corrections for elements in their standard states; the corresponding values were taken from the ATcT[26] and article by A. Nicolaides et al.[27]

For energetic salts, the solid-phase enthalpies of formation were calculated on the basis of the Born–Haber energy cycle by using the Jenkins–Glasser method.[28]

[21] M. J. Frisch, G. W. Trucks, H. B. Schlegel, G. E. Scuseria, M. A. Robb, J. R. Cheeseman, G. Scalmani, V. Barone, B. Mennucci, G. A. Petersson, H. Nakatsuji, M. Caricato, X. Li, H. P. Hratchian, A. F. Izmaylov, J. Bloino, G. Zheng, J. L. Sonnenberg, M. Hada, M. Ehara, K. Toyota, R. Fukuda, J. Hasegawa, M. Ishida, T. Nakajima, Y. Honda, O. Kitao, H. Nakai, T. Vreven, J. A. MontgomeryJr, J. E. Peralta, F. Ogliaro, M. Bearpark, J. J. Heyd, E. Brothers, K. N. Kudin, V. N. Staroverov, R. Kobayashi, J. Normand, K. Raghavachari, A. Rendell, J. C. Burant, S. S. Iyengar, J. Tomasi, M. Cossi, N. Rega, J. M. Millam, M. Klene, J. E. Knox, J. B. Cross, V. Bakken, C. Adamo, J. Jaramillo, R. Gomperts, R. E. Stratmann, O. Yazyev, A. J. Austin, R. Cammi, C. Pomelli, J. W. Ochterski, R. L. Martin, K. Morokuma, V. G. Zakrzewski, G. A. Voth, P. Salvador, J. J. Dannenberg, S. Dapprich, A. D. Daniels, Ö. Farkas, J. B. Foresman, J. V. Ortiz, J. Cioslowski and D. J. Fox, Gaussian 09, Revision D.01, Gaussian, Inc., Wallingford CT, **2013**.

[22] Werner, H.-J.; Knowles, P. J.; Knizia, G.; Manby, F. R.; Schutz, M.; Celani, P.; Korona, T.; Lindh, R.; Mitrushenkov, A.; Rauhut, G. et al. MOLPRO, version 2010.1, **2010**.

[23] L. A. Curtiss, P. C. Redfern, K. Raghavachari, Gaussian-4 theory, *J. Chem. Phys.*, 2007, **126**, 84–108. https://doi.org/10.1063/1.2436888

[24] Karton, A.; Martin, J. M. L. Explicitly correlated Wn theory: W1-F12 and W2-F12 J. Chem. Phys. 2012, 136, 124114. https://doi.org/10.1063/1.3697678

[25] L. A. Curtiss, K. Raghavachari, P. C. Redfern, J. A. Pople, Assessment of Gaussian-2 and density functional theories for the computation of enthalpies of formation, *J. Chem. Phys.*, 1997, **106**, 1063–1079.

[26] B. Ruscic, D. H. Bross, Active Thermochemical Tables (ATcT) values based on ver. 1.122e of the Thermochemical Network, Argonne National Laboratory, **2019**, available at ATcT.anl.gov.

[27] A. Nicolaides, A. Rauk, M. N. Glukhovtsev, L. Radom, Heats of Formation from G2, G2(MP2), and G2(MP2,SVP) Total Energies, *J. Phys. Chem.*, 1996, **100**, 17460–17464. https://doi.org/10.1021/jp9613753

[28] H. D. B. Jenkins, D. Tudela, L. Glasser, Lattice Potential Energy Estimation for Complex Ionic Salts from Density Measurements, *Inorg. Chem.* 2002, **41**, 2364–2367. https://doi.org/10.1021/ic011216k

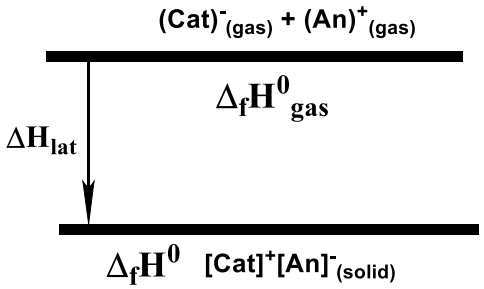

Fig. SIF14. The Born-Haber energy cycle for calculating enthalpies of formation of energeticsalts.

$$\Delta H_f^\circ(salt, 298\ K) = \Delta H_f^\circ(cation, 298\ K) + \Delta H_f^\circ(anion, 298\ K) - \Delta H_L \quad (2)$$

ΔH_L for salt M_pX_q can be predicted by using the formula suggested by Jenkins, et al.

$$\Delta H_L = U_{POT} + \left[p\left(\frac{n_M}{2} - 2\right) + q\left(\frac{n_X}{2} - 2\right)\right] RT = U_{POT} + 2RT \quad (3)$$

where n_M and n_X depend on the nature of the ions Mp^+ and Xq^- and are equal to 6 for nonlinear polyatomic ions. The equation for lattice potential energy U_{POT} (equation 4) has the form:

$$U_{POT}\ [\text{kJmol}^{-1}] = 2I[\alpha(V_m)^{-\frac{1}{3}} + \beta] \quad (4)$$

where I is the ionic strength of the lattice (I can be calculated as $I = \frac{1}{2}\sum n_i z_i^2$, where n_i is the number of ions of type i in the formula unit with charge z_i), V_m/nm^{-3} molecule^{-1} is the molecular (formula unit) volume obtained directly from crystal structure data using cell parameters, α (117.3 kJ mol^{-1} nm) and β (51.9 kJ mol^{-1} nm) are appropriate fitted coefficients chosen according to the stoichiometry of the salt.

Table SIF5. Calculated and experimental enthalpies of formation for compounds 2a,b, 3b,c and 6b,d

Salt	V_m nm^{-3}	U_{POT} kcal·mol^{-1}	ΔH_L kcal·mol^{-1}	ΔH_f°(Cat+An)[a] kcal·mol^{-1}	ΔH_f°(s)[b] kcal·mol^{-1}	ΔH_f°(s)[c] **kcal·mol^{-1}**	Inaccuracy of calculation method
2a	0.128	136.0	136.6	234.9 (241.1)	98.3 (104.5)	**83.1**	15.2 (21.4)
2b	0.144	131.6	132.2	266.6 (272.4)	134.4 (140.2)	**112.0**	22.4 (28.2)
3b	0.142	132.1	132.7	218.0 (222.2)	85.3 (89.5)	**78.6**	6.7 (10.9)
3c	0.155	129.0	129.7	249.7 (253.5)	120.0 (123.8)	**107.8**	12.2 (16.0)
6b	0.176	124.7	125.3	260.7 (272.0)	135.4 (146.7)	**119.6**	15.8 (27.1)
6d	0.185	123.2	123.8	292.4 (303.3)	168.6 (179.5)	**146.8**	*21.8 (33.1)*

[a] The sum of gas-phase formation enthalpies of the anions (**2**, **3**, and **6**) and the ammonium and hydrazinium cations calculated at the G-4 and W1-F12 (in brackets) level of theory using the atomization energy approach. [b] Enthalpy of formation in solid state. [c] Experimental enthalpy of formation obtained in this work except the one for salt **6d** (bold and red) which value was estimated

The data presented in the Table SIF5 shows the divergence between computed values of the enthalpies and the experimental ones. Both G-4 and W1-F12 methods overestimate the enthalpy of formation more than 15 kcal·mol^{-1} in case of salts **2a,b** and **6b** and more than 6 kcal·mol^{-1} in case of salts **3b,c**. We assume calculated enthalpy of salt **6d** also to be higher than the experimental one. Therefore, we decided to estimate the calculation error in order to obtain a more accurate enthalpy value. It can be seen that there is an approximate difference of 5–7 kcal·mol^{-1} between the calculation inaccuracies for hydrazine and ammonium salts, both for TF **2a,b** as well as TFO **3b,c**. We suppose that this value will also applicable to TFNA **6b,d**. We took the average value of 6 kcal·mol^{-1} to calculate the amount of overestimation for the G-4 and W1-F12 methods (italics in Table SIF5). Hence the estimated enthalpy of formation of hydrazinium salt **6d** is equal to 146.8 kcal·mol^{-1}.

pK_a measurement of TF 1

pK_a of TF **1** was measured in water using the spectrophotometric method in phosphate buffers.[29] A solution of TF **1** in dimethyl sulfoxide was added to a buffer solution with a certain pH value in a quartz cuvette (l = 1 cm), and then the absorption spectrum of the compound was recorded. It should be noted that at low concentrations of TF **1** ($c = 10^{-4}$ M) absorption of the dissociated form in the visible region was not observed, while at high concentrations ($c = 10^{-2}$ M) the undissociated H-form began to opalesce in buffer solutions with pH < 8.5. So correct optical density data could not be obtained. Nevertheless, we were able to estimate approximately the pK_a by the change from the colored solution to opalescence; the acidity of TF **1** can be assessed as $pK_a = 9$.

[29] Y. E. Zevatskii, D.V. Samoilov and N.O. Mchedlov-Petrosyan, Conthemporary methods for the experimental determination of dissociation constants of organic acids in solutions, *Russ J Gen Chem*, 2009, **79**(9), 1859–1889. https://doi.org/10.1134/S1070363209090138

Aromaticity

The availability of different salts and the presence of multiple crystallographically independent anions in the structures of some of them made it possible to conduct a detailed comparison of their geometric parameters. For simplicity, the heterocyclic part of the anions can be assumed to have C_{2v} symmetry in an isotropic crystallographic environment. Full data on bond lengths is provided in Table SIF2 and Fig SIF13 for numerical and visual representation, and averaged experimental bond lengths are listed in Table SIF6. For comparison, the latter contains also values calculated for isolated systems by the PBE0/def2-TZVP method. Note that in the DFT-optimized anions most discrepancies with experimental data are observed for polar bonds N–O of the furazan rings, those lengths are usually underestimated by DFT methods, and N–O/N–N bonds with exocyclic atoms, which are sensitive to crystal environment; other bond lengths are reproduced relatively well.

Table SIF6. Bond lengths (Å) in studied compounds, averaged for equivalent bonds of the anion in the approximation of C_{2v} symmetry of the bicyclic anion, and for crystallographically independent molecules in 2b and 3b.

	X-ray			PBE0/def2-TZVP			PBE0/def2-TZVP		
	TF anion	TFO anion	TFNA anion	TF anion	TFO anion	TFNA anion	TF **1**	TFO **5**	TFNA **10**
N1–O2/	1.407	1.417	1.402	1.379	1.388	1.376	1.379	1.382	1.350
O2–N3	—	—	—	—	—	1.374	1.348	1.360	1.355
N1–C6A/	1.311	1.307	1.314	1.307	1.302	1.306	1.299	1.291	1.314
N3–C3A	—	—	—	—	—	1.307	1.303	1.298	1.314
C3A–N4/	1.365	1.366	1.362	1.357	1.349	1.348	1.350	1.352	1.348
N6–C6A	—	—	—	—	—	1.348	1.377	1.366	1.348
N4–N5/	1.342	1.355	1.337	1.330	1.352	1.334	1.366	1.407	1.312
N5–N6	—	—	—	—	—	1.330	1.272	1.296	1.323
C3A–C6A	1.405	1.418	1.411	1.418	1.423	1.416	1.404	1.410	1.412
N5–O_{ex}/N_{ex}	—	1.259	1.377	—	1.225	1.332	—	1.205	1.362

It should be mentioned that, on the one hand, the experimental geometric parameters vary in a relatively wide range for anions of the same type, with some differences being higher than the estimated standard uncertainty for each bond. These differences can be the result of H-bonding, bond polarization due to intermolecular interactions in general, and possibly different total amount of charge transfer between the ions. On the other hand, despite the chemical difference in the nature of the substituent at atom N-5, the geometry of all the anions remains very similar, and we can

only notice some trends. Thus, N–C bonds are virtually insensitive to the presence of the exocyclic substituent. In the case of a polar N–O bond of the furazan and an N–N bond of the triazole cycles, there is a tendency of the experimental bond lengths in anion of TFO to be systematically longer than in anions of TF and TFNA, which is consistent with the DFT data.

As the geometric parameters for all anions are similar, it was interesting to compare electronic characteristics of the anions, as well as H-forms **1**, **5** and **10**, those data are unfortunately unavailable due to their low stability. We have calculated geometry-based Bird's[30] HOMA[31] and HOMHED[32] and magnetic NICS(1)zz aromaticity indices (Table SIF7), based on PBE0/def2-TZVP wavefunctions.

Table SIF7. Aromaticity indices of the anions and neutral forms of the compounds studied.[a]

	X-ray			PBE0/def2-TZVP			PBE0/def2-TZVP		
	anion of						H-form		
	TF	TFO	TFNA	TF	TFO	TFNA	**1**	**5**	**10**
					Furazan ring				
HOMA	0.39	0.27	0.41	0.54	0.45	0.56	0.64	0.57	0.70
HOMHED	0.69	0.62	0.72	0.80	0.75	0.81	0.84	0.80	0.90
Bird	39	35	42	50	45	51	52	48	62
$NICS(1)_{zz}$	–32.3	–28.2	–31.7 –32.1	–33.9	–29.6	–32.5 –32.5	–33.8	–30.3	–36.8 –36.9
					Triazole ring				
HOMA	0.89	0.81	0.90	0.91	0.83	0.9	0.83	0.72	0.96
HOMHED	0.94	0.90	0.95	0.96	0.92	0.97	0.90	0.84	0.98
Bird	82	85	86	90	88	92	69	69	91
$NICS(1)_{zz}$	–24.9	–17.8	–23.6 –23.7	–26.5	–19.2	–23.6 –24.1	–23.8	–15.8	–30.0 –31.0

[a] The indices based on experimental data are calculated using the averaged bond lengths taken from Table SIF6. NICS(1)zz values were calculated for the averaged experimental geometry to show their low dependency on the geometry.

Immediately apparent is the discrepancy between the geometry-based and magnetic indices for the furazan ring. While the Bird index is generally unreliable for complex heterocycles, the

[30] C. W. Bird, A new aromaticity index and its application to five-membered ring heterocycles, *Tetrahedron*, 1985, **41**(7), 1409–1414. https://doi.org/10.1016/S0040-4020(01)96543-3

[31] T. M. Krygowski, Crystallographic studies of inter- and intramolecular interactions reflected in aromatic character of π-electron systems, *J. Chem. Inf. Comput. Sci.*, 1993, **33**(1), 70–78. https://doi.org/10.1021/ci00011a011

[32] C. P. Frizzo and M. A. P. Martins, Aromaticity in heterocycles: new HOMA index parametrization, *Struct. Chem.*, 2012, **23**, 375–380. https://doi.org/10.1007/s11224-011-9883-z

inconsistency between the original HOMA index and NICS(1)$_{zz}$ is important. The highly negative values of NICS(1)$_{zz}$ values of *ca.* –30 suggest a high aromaticity comparable to the benzene molecule, whereas HOMA values of 30–40 are more typical for compounds with much less effective cyclic delocalization. In fact, this inconsistency stems from a well-known problem of HOMA to underestimate the aromaticity of 5-membered rings containing an oxygen atom, such as furan and isomeric oxazoles,[33] as the "optimal" C–O and N–O distances of 1.265 and 1.248 Å are too short for such rings (compare to N–O of about 1.4 Å in our anions). The use of alternative parameterization of the HOMA index, HOMHED, leads to significantly higher values that are probably still lower than expected from NICS(1)$_{zz}$. However, it is important that both HOMA-based indices and NICS(1)$_{zz}$ values follow the same trends in the series of anions and H-forms discussed below.

Taking into account the above, both heterocyclic components of anions of TF, TFO and TFNA and their parent H-forms **1**, **5**, and **10** can be classified as aromatic. The aromaticity of furazan ring is somewhat lower for experimental geometry of the anions, apparently due to longer N–O bonds.

If we compare anions in terms of aromaticity, it is apparent that cyclic delocalization in anions TF and TFNA is very similar for both rings, while the aromaticity of the rings in anion of TFO is reduced in terms of all indices. The triazole ring is more sensitive to the presence of *N*-oxide atom than the furazan ring, since, for example, the NICS(1)$_{zz}$ value for DFT-optimized geometry in anion of TFO is reduced by 28% for the former and by 13 % for the latter, as compared to anion of TF. It can be supposed that the electron-withdrawing *N*-oxide atom reduces the amount of electron density available for delocalization thus reducing its effectiveness. The same reduction of aromaticity was observed by us for 1,2,3,4-tetrazine 1,3-dioxides.[34] In contrast, despite formal polarity of the N-5–N-7 bond in anion of TFNA, delocalization in the triazole ring is nearly as effective as in anion of TF.

Comparing H-forms, we should take into account that for the molecules corresponding to anions of TF and TFNA, there are actually two different possible attachment points of the H atom

[33] A. Mrozek, J. Karolak-Wojciechowska, P. Amiel and J. Barbe, Five-membered heterocycles. Part I. Application of the HOMA index to 1,2,4-trizoles, *J. Mol. Struct.*, 2000, **524**, 151–157. https://doi.org/10.1016/S0022-2860(99)00459-7

[34] A. A.Voronin, A. M. Churakov, M. S.Klenov, Y. A. Strelenko, I. V. Fedyanin and V. A. Tartakovsky, Synthesis of 1,2,3,4-Tetrazine 1,3-Dioxides Annulated with 1(2)-Aryl-1,2,3-triazoles. *Eur. J. Org. Chem.*, 2017, **33**, 4963–4971. https://doi.org/10.1002/ejoc.201700750

(the furazan N atoms are not considered). However, according to calculations with the PBE0/def2-TZVPP method, the H-form **1** with the H atom bonded to N-5 rather than to N-4 is by 4.3 kcal/mol higher in energy, and H-form **10** with the H atom attached to the nitroimide atom N-7 is by 5.1 $kcal \cdot mol^{-1}$ more favorable than the one with the H atom attached to the N atom of the triazole ring. Therefore, chemical nature of the H-form **10**, is different from H-forms **1** and **5**, and so should be the electronic structure.

The differences are reflected in the molecular geometry. The most significant changes in molecules **1** and **5** are, of course, observed for N–N bonds of the triazole fragments, which are equated in the corresponding anions of TF and TFO. In H-forms the N–N bond adjacent to the NH group becomes almost single, and the second nearly double, in agreement with the canonical structures depicted in Schemes 1 and 2. The increase in bond length alternation propagates to other bonds in the molecule, primarily on the non-protonated side of the molecule. In contrast, bond length alternation in H-form **10** is even less pronounced than in anion of TFNA, as N–O bonds of the furazan ring are shortened, and only one of the N–N bonds of the triazole is also shortened.

Therefore, the absence of an H atom attached to the triazole atom and the presence of the nitramine NH in **10** hardly interfere with the cyclic delocalization. Indeed, the molecule **10** turns out to be the most aromatic system among all H-forms and anions, and this is true for both heterocyclic moieties. As the formation of the anion of TFNA reduces the aromaticity of both rings, molecule **10** is expected to be a relatively weak acid, although its acidity cannot be directly compared with that of compounds **1** and **5** from a structural viewpoint. In contrast to H-form 10, the aromaticity of molecules **1** and **5** is less than that of their anions, and the difference is more pronounced for the triazole ring having exocyclic H atom in the H-form. The decrease of the cyclic delocalization in **5** is so pronounced, that the DFT-optimized planar conformation is a saddle point with an imaginary frequency of 104 i cm^{-1} corresponding to the pyramidalization of the protonated atom N-4. On the other hand, the planar geometry of **1** corresponds to an energy minimum. Therefore, molecule **5** seems to benefit more than **1** from the formation of the anion, which can explain its much lower pK_a values of *ca. 2,* comparable to strong inorganic acids instead of pK_a (TF 1) ~ 9.

Hirshfeld surfaces an 2D fingerprint plots

	2a	2b	3b	3c	6b
	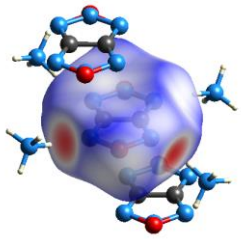	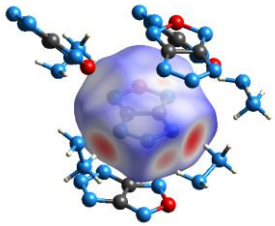	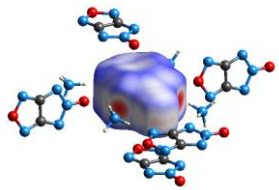	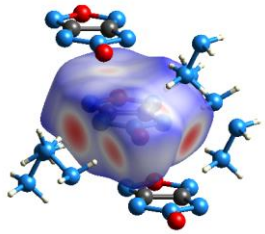	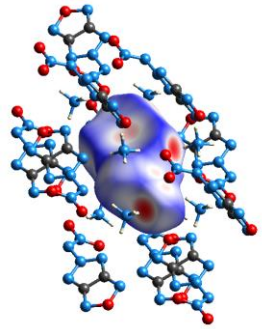
C-C	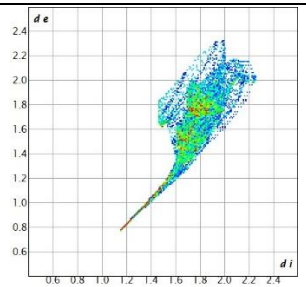	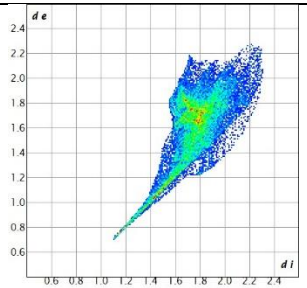	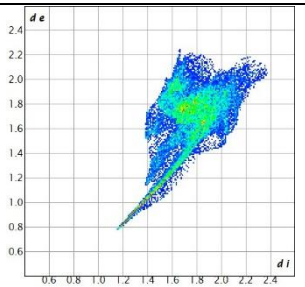	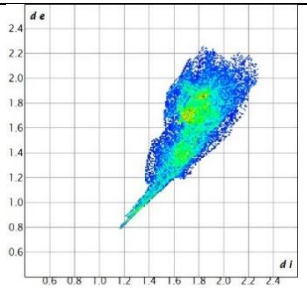	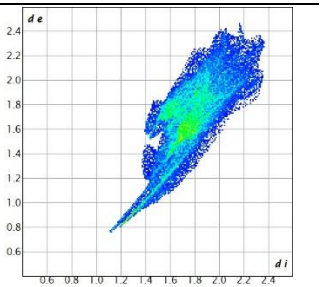
	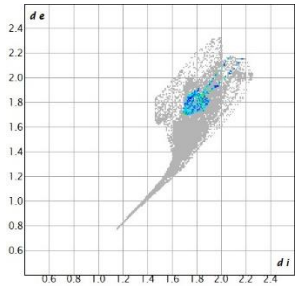	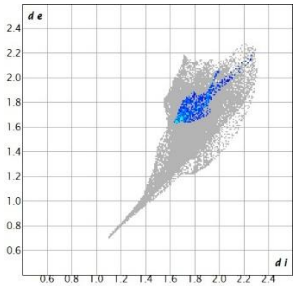	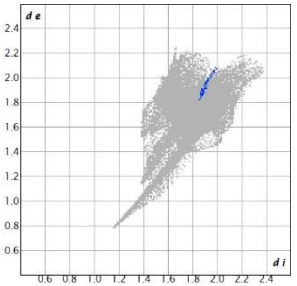	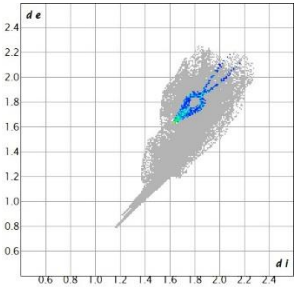	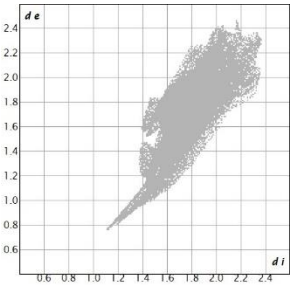

N-N

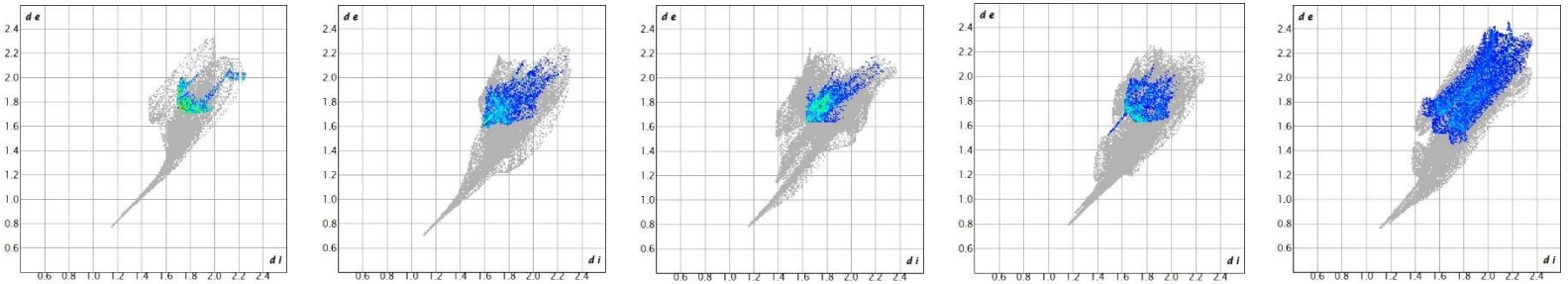

O-O

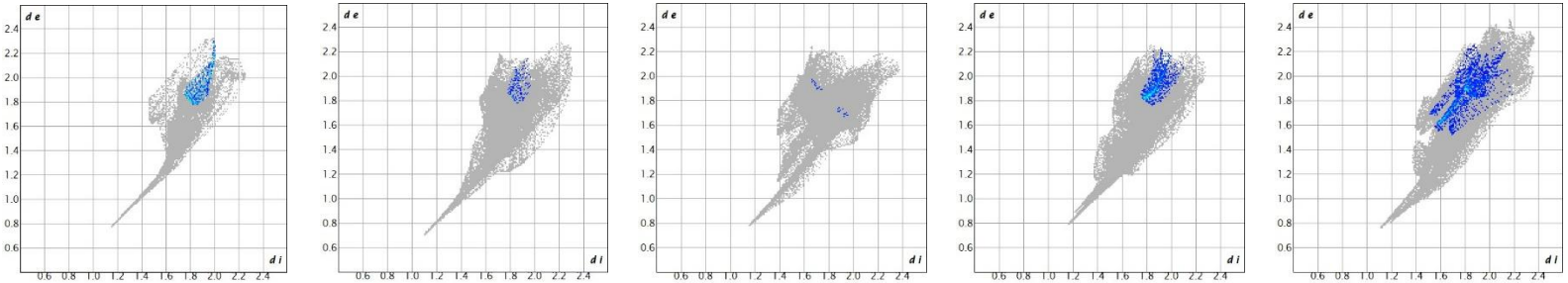

C-H

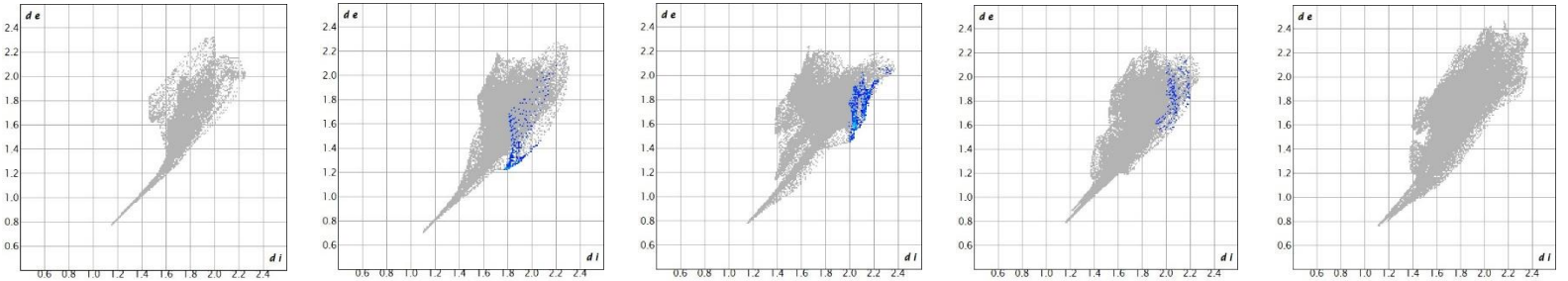

N-H

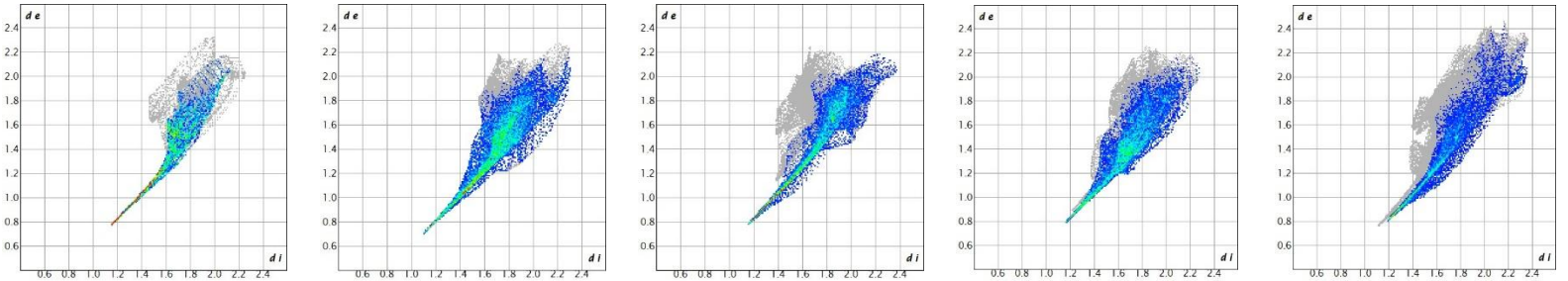

O-H

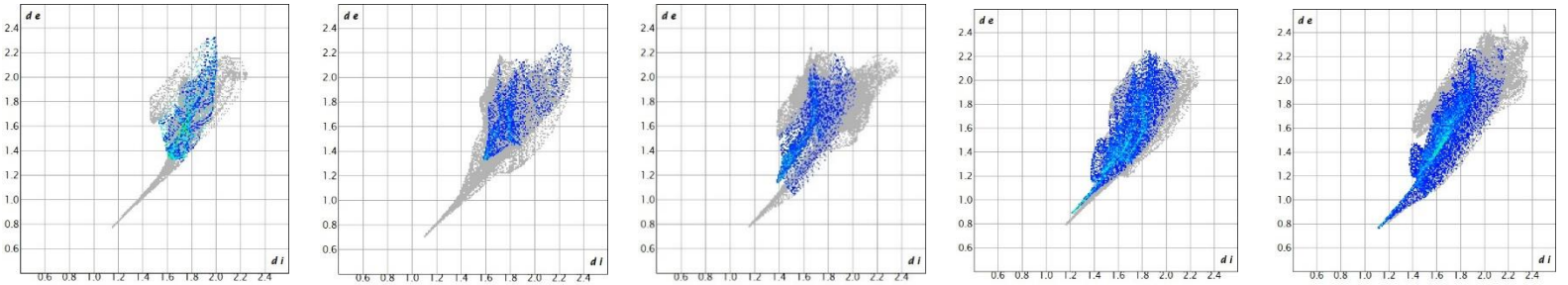

C-N

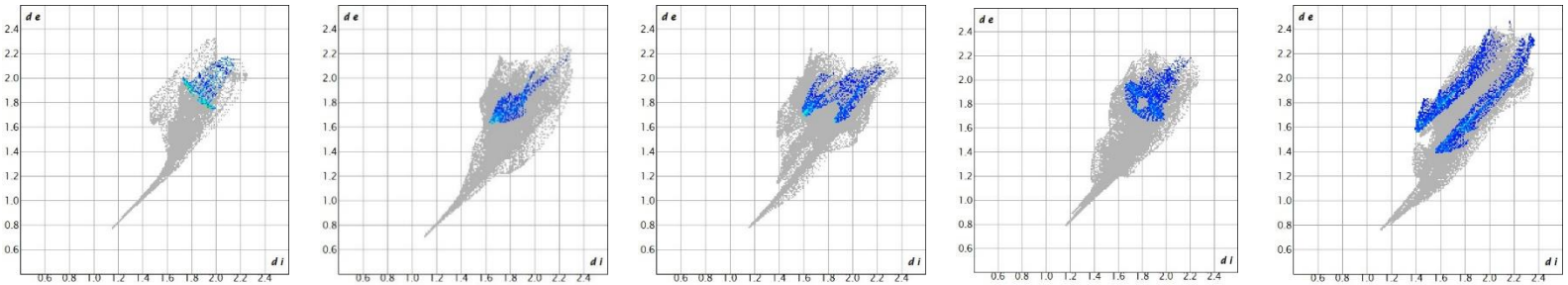

C-O

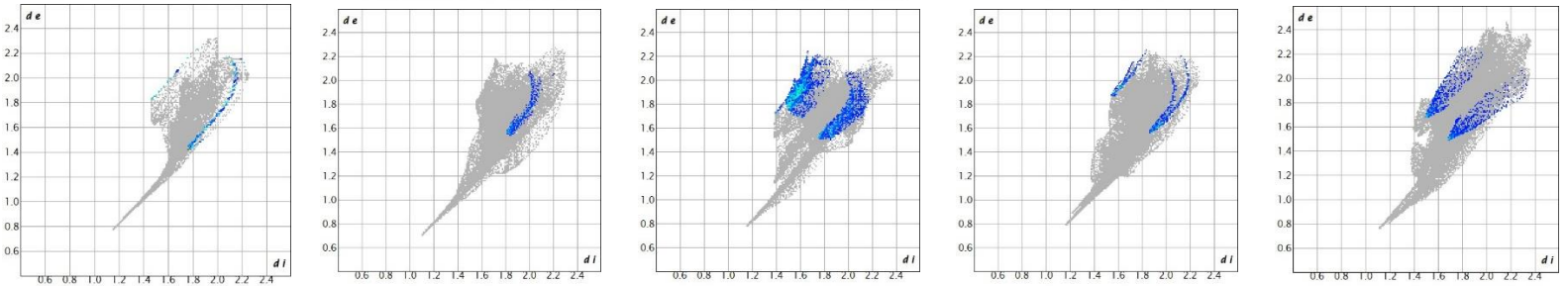

N-O

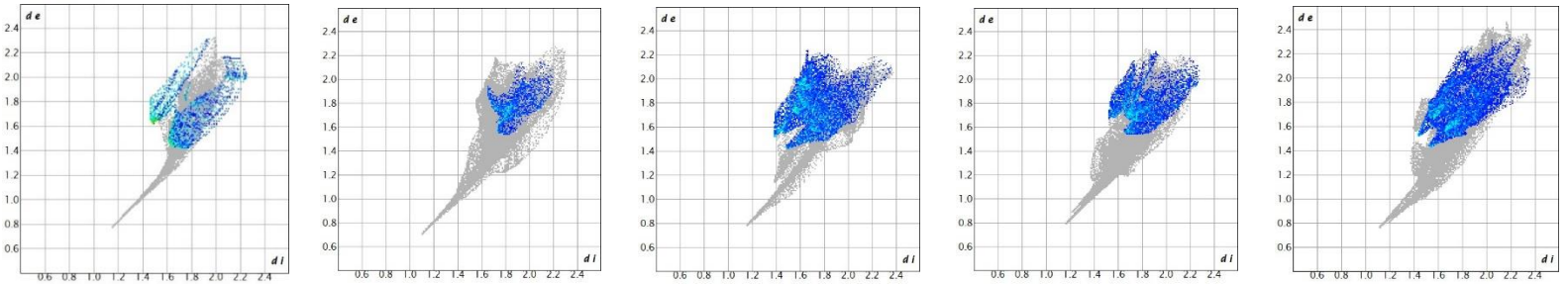

Surface morphology analysis

We have taken a look at the morphology of samples of new salts **2a,b** and **6b** (Fig. SIF15), since the dependence of the sensitivity to mechanical stress on the size and shape types of particles was noticed.[35] Sample **2a** are needles with a thickness of approximately 10–60 μm and a smooth surface were observed, while sample **2b** are prismatic particles with a size of 0.2–1.0 mm with a developed surface morphology. Sample **6b** consists of agglomerates of particles with a size of ~2–6 μm and as it could be seen the surface of these salt is very developed.

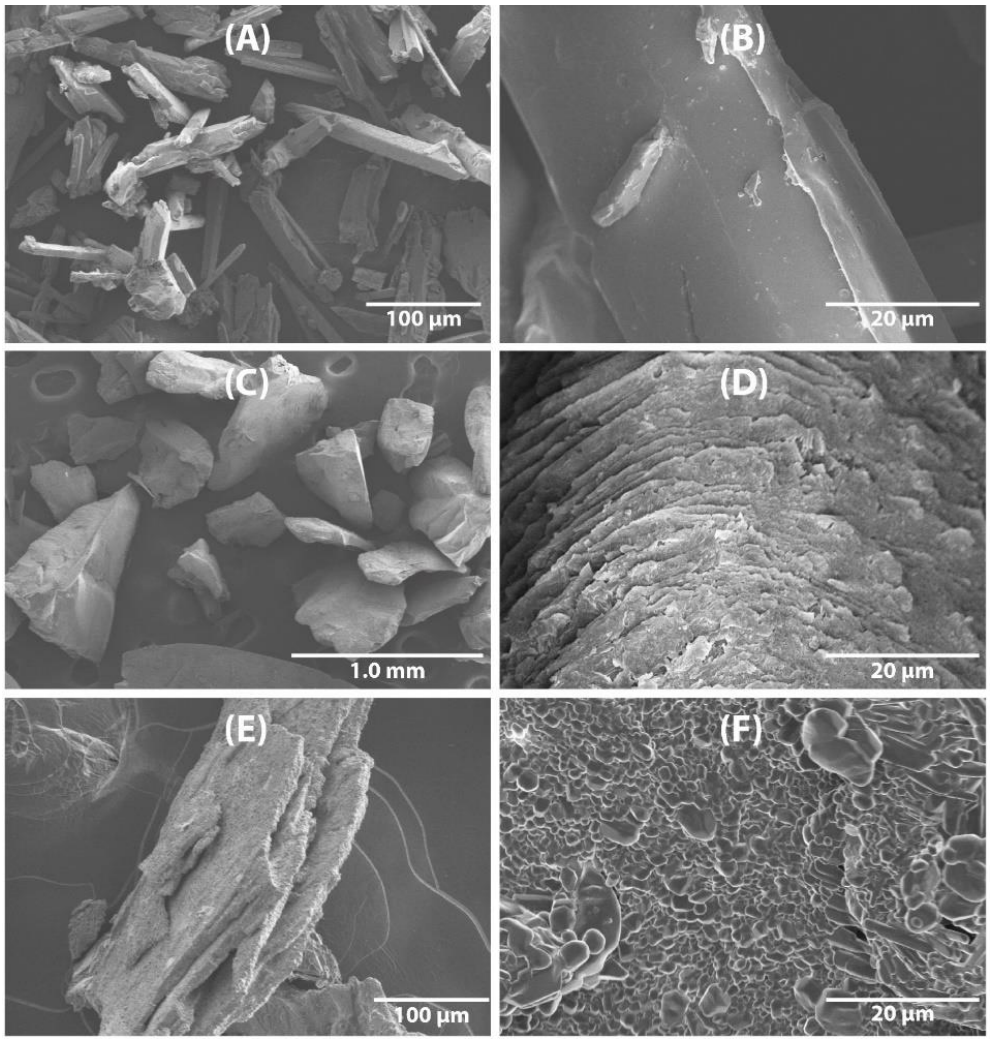

Fig. SIF15. SEM images of **2a** (A, B), **2b** (C, D), **6b** (E, F).

[35] N. V. Muravyev, D. B. Meerov, K. A. Monogarov, I. N. Melnikov, E. K. Kosareva, L. L. Fershtat, A. B. Sheremetev, I. L. Dalinger, I. V. Fomenkov and A. N. Pivkina, Sensitivity of energetic materials: Evidence of thermodynamic factor on a large array of CHNOFCl compounds, *Chemical Engineering Journal*, 2021, **421**(1): 129804. https://doi.org/10.1016/j.cej.2021.129804